Fluids in narrow pores: Adsorption, capillary condensation, and critical points

R. Evans and U. Marini Bettolo Marconi
H. H. Wills Physics Laboratory, University of Bristol, Bristol BS8 1TL, United Kingdom

P. Tarazona
Instituto de Fisica del Estado Solido, Facultad de Ciencias, Universidad Autonoma, Madrid 28049, Spain

(Received 22 July 1985; accepted 3 September 1985)

By means of a density functional approach the phase equilibria of a simple fluid confined by two adsorbing walls have been investigated as a function of wall separation H and chemical potential μ for temperature T corresponding to both partial and complete wetting situations. For large values of H and small undersaturations $\Delta\mu \equiv \mu_{sat} - \mu$, we recover the macroscopic formulas for the undersaturation at which a first order phase transition (capillary condensation) from dilute "gas" to a dense "liquid" occurs in a single, infinitely long slit. For smaller H we compute the lines of coexistence between gas and liquid in the $(\Delta\mu, 1/H)$ plane at fixed values of T. The adsorption $\Gamma(\Delta\mu)$, at fixed T and H, is characterized by a loop. At the first order transition Γ jumps discontinuously by a finite amount; however metastable states exist and these could give rise to hysteresis of the adsorption isotherms obtained for the single slit. The loop disappears at a capillary critical point $(\Delta\mu_c, 1/H_c)$ at each T. For $H < H_c$, or $\Delta\mu > \Delta\mu_c$, condensation can no longer occur and no metastable states are present. The location of the critical points is described and for a complete wetting situation we find that these lie outside the bulk two phase region. Our theory provides a simple explanation of phase transitions observed in earlier computer simulations and mean-field lattice gas calculations for confined fluids and suggests that measurements of the forces between plates, either by simulation or in real fluids, should provide rather direct information about capillary condensation and, possibly, capillary critical points. The relevance of our results for adsorption experiments on mesoporous solids is discussed briefly.

I. INTRODUCTION

Capillary condensation is the name given to the phenomenon whereby a fluid whose chemical potential, or pressure, is less than its value at saturation and is, therefore, a gas in *bulk*, condenses to form a dense liquid-like state inside a narrow capillary or in the pores of a solid. A physicist might view this phenomenon as a shift of the bulk coexistence curve (line of first order transitions) arising from confinement of the fluid. Chemists have long used the notion of capillary condensation to interpret the measured adsorption isotherms of gases in mesoporous solids.[1] These are characterized by steeply varying portions and pronounced hysteresis loops (see Fig. 1). The rising part (adsorption) is associated with condensation while the decreasing part (desorption) is associated with evaporation of the condensed liquid. Zsigmondy[2] appears to have been the first to apply the macroscopic Kelvin equation to the interpretation of such data. This equation relates the relative pressure p/p_{sat} of gas in equilibrium with a liquid meniscus to the mean radius of curvature R_m of that meniscus

$$k_B T(\rho_l - \rho_g)\ln(p_{sat}/p) = 2\gamma_{lg}/R_m,$$

where ρ_l and ρ_g are the number densities of coexisting liquid and gas and γ_{lg} is the liquid–gas surface tension at temperature T. Condensation, or more frequently, evaporation of the fluid in the pore is assumed to occur when the bulk pressure p satisfies this equation. Indeed the Kelvin equation is often used to infer the pore radius from the measured isotherms.[1] Such a procedure is beset with difficulties. Should the equation be applied to the adsorption or desorption branch? Is it valid when wetting films develop? Does the first order transition persist to very small radii or is there a capillary critical point? How should one take into account the nonuniformity of pore size? What is the origin of hysteresis? There is a large literature[1,3] describing attempts to answer such questions and to provide a more satisfactory theory of adsorption and capillary condensation in narrow pores. We mention below what we believe are the more relevant contributions, concentrating on the idealized case of a single, infinitely long, model capillary.

Cohan[4] proposed a modification to the Kelvin equation which allowed for the presence of thick wetting films intruding between the gas and the walls of the capillary. In the absence of wetting films, corresponding to contact angle $\theta > 0$, the mean radius of curvature of the meniscus R_m is taken to be $H/\cos\theta$ or $R/\cos\theta$ for a slit or cylinder, respectively.[1] Here H is the separation of the parallel walls and R is the interior radius of the cylinder. When $\theta = 0$ wetting films of thickness t develop and Cohan argued that the effective mean radius of curvature of the cylindrical meniscus in the slit should be reduced to H-$2t$ and that of the hemispherical meniscus in the cylinder to R-t. A more systematic treatment of the influence of wetting films on capillary condensation was contained in a remarkable pioneering paper published by Derjaguin[5] in 1940 who showed that the correction to the Kelvin equation depends on the form assumed for the attractive part of the solid–fluid potential function; replacing H by H-$2t$ or R by R-t, is not generally valid.[6] The significance of

 0021-9606/86/042376-24$02.10

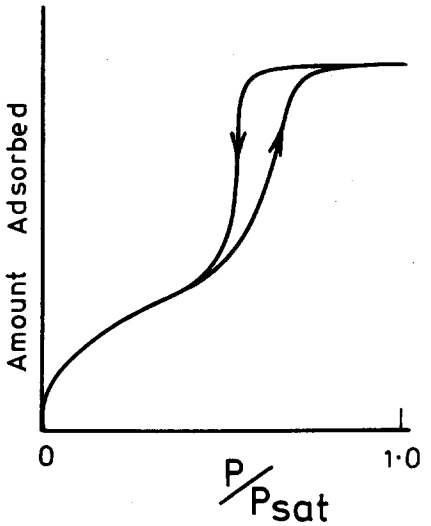

FIG. 1. A typical adsorption isotherm for a mesoporous solid. The rising part of the hysteresis loop corresponds to adsorption while the decreasing part corresponds to desorption. Isotherms of this type (Ref. 1) are often referred to as type IV.

Derjaguin's paper does not seem to be recognized in the Western literature. Most subsequent attempts[1,3,7–9] at improvements on the Kelvin equation have either ignored or failed to make direct connection with Derjaguin's results and, consequently, the status of the subsequent theories remains somewhat obscure. This work was, in the main, based on macroscopic or semimacroscopic concepts. Microscopic theories, based on lattice models of the adsorbed fluid, were developed by Hill[10] and Nicholson.[11] Hill[10] studied the adsorption between two parallel walls using a generalization of the well-known B.E.T. treatment and obtained isotherms characterized by loops. He showed that a first-order transition, corresponding to capillary condensation, was associated with a jump in adsorption from one branch of the loop to another. Hill also proposed a mechanism for the observed hysteresis of the isotherms which involved metastable portions of the calculated loops. Nicholson[11] performed detailed mean-field calculations for a lattice gas confined in a single cylindrical capillary and found jumps in the adsorption isotherms for large radii and small undersaturations which could be attributed to capillary condensation. For small radii the adsorption increased monotonically with increasing $p/p_{\rm sat}$. Neither paper appears to have made significant impact on the subject but we consider these to be important contributions. Similar remarks apply to the paper by Derjaguin and Churaev[12] who discussed the behavior of wetting films and their effect on adsorption and condensation in a slit-like capillary.

Computer simulations might be expected to shed some light on these phenomena. There are two simulations which are directly relevant. Very recently van Megen and Snook[13] observed jumps in the adsorption isotherms in grand canonical Monte Carlo calculations performed for an undersaturated Lennard-Jones fluid confined in a slit-like capillary. They interpreted their results in terms of condensation to a liquid, but did not attempt to relate them to the classical formula for capillary condensation. Earlier simulations by Lane and Spurling[14,15] for the same type of model system computed the adsorption, density profiles, and other properties as a function of H the separation of the walls. At a certain separation these authors found a first order transition from a gas configuration, stable at large H, to a dense liquid configuration, stable at small H. They termed this "a new type of surface transition." Freasier and Nordholm[16] have carried out density functional calculations for the same model and found the same transition. We shall see in Sec. III that the results of Refs. 14–16 are consistent with "conventional" capillary condensation; the observed transition is well described by a simple theory which makes strong appeal to macroscopic arguments.

During the last few years several theoretical papers have been concerned with the phase equilibria of fluids, or magnets, between parallel plates. A large fraction of these deal with critical point shifts, i.e., the shift and modification of bulk critical behavior resulting from the finite thickness of the sample and from interactions between the fluid and the plates. Mean-field theory, in discrete and continuum versions, has been applied to the three dimensional problem and powerful scaling theories exist.[17] Nakanishi and Fisher[17] address themselves to the general problem of critical points in confined Ising/lattice-gas models, but they do not make contact with earlier work on capillary condensation so the significance of their results for adsorption in pores is not immediately apparent. A few authors have discussed the shift of the bulk coexistence curve in terms of Landau theory.[18–20] Chalupa and Huberman[18] speculate on the nature of the capillary phase diagram but do not present any detailed results. Lipowsky and Gompper[19] derive an expression for the shift in the coexistence curve at large H. Although they do not recognize it, their result[19] is equivalent to the Kelvin equation. These authors also make some important remarks about the thickness of wetting films in capillaries and on the presence of metastable states. Sornette[20] derives a similar result for the shift of the first order transition and argues that for H smaller than some critical value no transition should occur. Again no attempt is made to connect the results with earlier macroscopic arguments. Finally we should note that Sheng[21] has calculated phase diagrams for models of nematic liquid crystals confined by parallel walls. The first order transition between nematic and paranematically ordered phases is shifted by confinement and critical points arise at small H. Sheng does not relate his results to capillary condensation.

The purpose of this lengthy introduction has been to show that, in spite of its importance for adsorption experiments in porous solids, the phase equilibria of fluids in narrow capillaries remains poorly understood. Researchers in one branch appear to be unaware of closely related work in other branches of physics and chemistry. Given the current upsurge of interest in the statistical mechanics of inhomogeneous fluids[22] and its applications to adsorption and wetting phenomena[23] it would seem appropriate to bring some of the more modern theoretical techniques to bear on this problem. In this paper we present some results of a study of the possible phase equilibria of a simple model fluid confined by two adsorbing parallel walls. Our theory is based on a mean-field density functional approach introduced original-

ly by Sullivan[24,25] in his studies of adsorption and wetting at the interface between a fluid and a single wall. While this approach gives a rather crude description of correlations in a bulk liquid it has provided a great deal of insight[23] into the various factors that determine adsorption isotherms and the systematics of wetting transitions. We shall see that the extension of the theory to the two-wall case provides new insight into the physics of capillary condensation, critical points, and the nature of adsorption in narrow pores. The theory has the merit of yielding useful (approximate) analytical results as well as being very well suited to numerical work. These features are especially advantageous when one is attempting to calculate a complete capillary phase diagram.

Our paper is arranged as follows: In Sec. II some general considerations concerning phase equilibria of fluids confined in a slit are presented. Derivations of the macroscopic Kelvin and Cohan equations are given and analogies made between bulk liquid–gas coexistence and coexistence in a capillary. The concept of a capillary critical point is introduced. Section III describes the theory. In Sec. III A the extension of Sullivan's approach to two walls is described and the differential equation for the density profile of the fluid is derived. A graphical construction for determining possible solutions is presented in Sec. III B. Wetting films arise naturally in our analysis. For a given wall separation H, at fixed chemical potential μ and temperature, different solutions, corresponding to liquid and gas configurations may exist. The solution with the lowest interfacial free energy $\gamma(H)$ is the equilibrium one. The procedure for calculating $\gamma(H)$ is described in Sec. III C. Capillary critical points and spinodals are analysed in Sec. III D; the divergence of the local compressibility and the implications for critical transverse correlations are also discussed here. In Sec. III E the form of the adsorption isotherms for fixed H is described; these exhibit loops. At a first order transition, the adsorption Γ jumps in a characteristic fashion, whereas at a critical point Γ remains continuous but $(\partial\Gamma/\partial\mu)_{H,T}$ diverges. We also consider the adsorption and the force on the walls as functions of H at fixed μ and T. This allows us to make contact with the simulations of Lane and Spurling[14,15] mentioned above. Our theory provides a direct physical explanation of their results and makes specific predictions for the variation of various properties at first order and critical transitions.

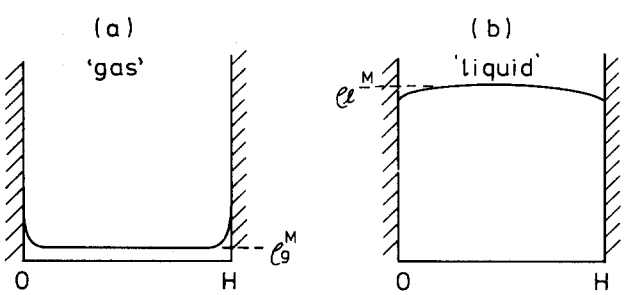

FIG. 2. Schematic density profiles $\rho(z)$ for (a) gas and (b) liquid configurations in a partial wetting situation. ρ_g^M and ρ_l^M are the densities at midpoint $z = H/2$.

Section IV contains the results of numerical calculations of adsorption isotherms for various separations H in both partial and complete wetting situations. Results for capillary phase equilibria, plotted as H vs pressure isotherms,[26] are presented for a specific choice of fluid–fluid and solid–fluid potentials. The trajectories of the lines of critical points are shown to be accounted for, approximately, by a simple slab approximation for the density profiles. We conclude in Sec. V with a discussion of our results and their possible relevance for adsorption and other experiments. Appendices A and B contain the derivations of equations that determine capillary spinodals and critical points.

II. GENERAL CONSIDERATIONS

We consider a model capillary consisting of two parallel adsorbing walls located at $z = 0$ and $z = H$ and unbounded in the x and y directions. The system is in contact with a reservoir of fluid at temperature T and chemical potential μ. For a given wall separation H the fluid in the slit will adopt the configuration that minimizes the grand potential $\Omega(\mu,H,T)$. It is convenient to divide Ω into a bulk and surface contribution

$$\Omega = -pV + \gamma(H)A_{sf}, \tag{1}$$

where p is the (bulk) pressure corresponding to the state (μ,T), A_{sf} is the total area of the solid–fluid interface, $V = HA_{sf}/2$ is the interior volume of the slit, and $\gamma(H)$ is the interfacial free energy per unit area. We suppose $T < T_c$, the bulk critical temperature, and $\mu < \mu_{sat}$, the chemical potential at saturation, so that the fluid is gas in bulk. The case

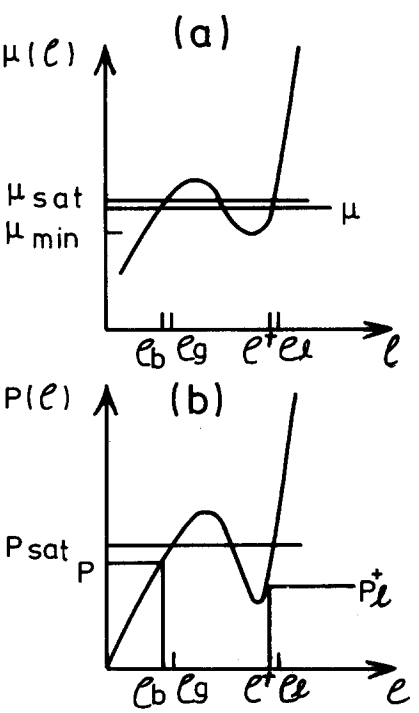

FIG. 3. Schematic plots of (a) the chemical potential and (b) the pressure of the bulk fluid as a function of density ρ at fixed $T < T_c$. We consider a fluid with $\mu < \mu_{sat}$ at pressure p and with density ρ_b. The metastable liquid with the same chemical potential has density ρ^+ and pressure $p_l^+ < p$. ρ_l and ρ_g are the densities of coexisting gas and liquid, respectively. If $\mu < \mu_{min}$ there is no metastable liquid.

$\mu > \mu_{sat}$, corresponding to a liquid in bulk, will be mentioned later.

In the limit $H \to \infty$, the phase equilibria of the fluid will be determined by *macroscopic* considerations. For sufficiently large H we may envisage a gas configuration [see Fig. 2(a)] which is, essentially, a superposition of two semi-infinite solid–gas configurations. If the undersaturation $\Delta\mu \equiv \mu_{sat} - \mu$ is small $\gamma(H) \approx \gamma_{sg}$, the solid–gas interfacial tension defined for $\mu = \mu_{sat}$ and $H = \infty$. The grand potential of such a configuration is then given by

$$\Omega_g \approx -pV + \gamma_{sg} A_{sf}.$$

If the walls exert sufficiently attractive forces on the molecules of the fluid, and $\Delta\mu$ is not too large, the fluid in the slit may condense to a liquid configuration [Fig. 2(b)] for which $\gamma(H) \approx \gamma_{sl}$, the solid–liquid interfacial tension again defined for $\mu = \mu_{sat}$ and $H = \infty$. The corresponding grand potential is

$$\Omega_l \approx -p_l^+ V + \gamma_{sl} A_{sf}. \tag{2}$$

Here p_l^+ is the pressure of the liquid that has condensed in the slit. Since the chemical potential μ is constant (equal to that of the reservoir) p_l^+ is the pressure of the *metastable* bulk liquid with density ρ_l^+ at the same value of μ. This argument clearly requires a van der Waals loop in the (bulk) μ vs ρ relation (see Fig. 3). A first-order phase transition from one configuration to the other will occur when $\Omega_g - \Omega_l = 0$, or when the pressure p satisfies

$$p - p_l^+ = (\gamma_{sg} - \gamma_{sl}) A_{sf}/V.$$

Introducing Young's equation for the contact angle θ at a single wall

$$\gamma_{sg} = \gamma_{sl} + \gamma_{lg} \cos\theta, \tag{3}$$

the last equation reduces to

$$p - p_l^+ = 2\gamma_{lg} \cos\theta / H, \tag{4}$$

where γ_{lg} is the liquid–gas surface tension at temperature T. For values of p smaller, or values of H larger, than those given by Eq. (4) the gas is the stable configuration, whereas for larger values of p or smaller values of H liquid is stable. The two configuration coexist when Eq. (4) is satisfied. All the quantities appearing in Eq. (4) are macroscopic (thermodynamic). Indeed the right-hand side is simply the macroscopic pressure difference that would arise across the concave cylindrical meniscus between liquid and gas in a vertical slit; the mean radius of curvature entering Laplace's formula is $H/\cos\theta$.

For small undersaturations p and p_l^+ can be expanded about p_{sat} and, to first order in $\Delta\mu$, $p - p_l^+ = \Delta\mu(\rho_l - \rho_g)$, where ρ_l and ρ_g are the number densities of coexisting liquid and gas (see Fig. 3). Equation (4) reduces to the more familiar Kelvin equation for the pressure at which condensation occurs if we make the additional assumption that the gas is close to ideal so that

$$\Delta\mu \approx k_B T \ln(p_{sat}/p) = 2\gamma_{lg} \cos\theta / H(\rho_l - \rho_g). \tag{5}$$

This derivation differs from the conventional argument[1] which invokes directly the pressure difference across a curved meniscus. Our treatment clarifies the status of the Kelvin equation; this should constitute a rigorous asymptotic result for the condensation pressure in the limits $H \to \infty$ and $\Delta\mu \to 0$, provided the bulk gas is sufficiently dilute to be treated as ideal. We remark that it is not necessary to introduce a meniscus into the problem nor is it necessary to make specific assumptions about solid–fluid contributions to the grand potential. The latter are included via the interfacial tensions γ_{sg} and γ_{sl}. For smaller H and larger $\Delta\mu$, $\gamma(H)$ will differ significantly from γ_{sg} or γ_{sl} and Eqs. (4) and (5) will become less accurate. Indeed it is of considerable interest to determine the regime of validity of these asymptotic results.

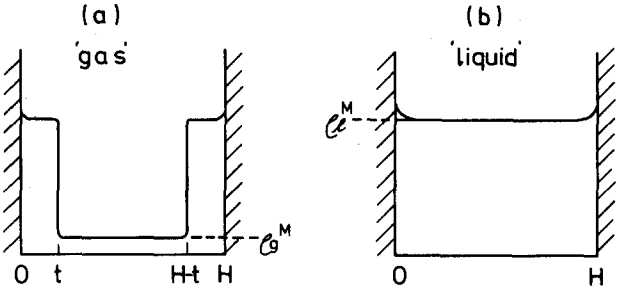

FIG. 4. Schematic density profiles $\rho(z)$ for (a) gas and (b) liquid configurations in a complete wetting situation. The gas has wetting films of thickness t at each wall. ρ_g^M and ρ_l^M are the densities at midpoint $z = H/2$.

The situation we have described above corresponds to partial wetting, i.e., $\theta > 0$. In the limit $\Delta\mu \to 0$ only a thin (microscopic) film of liquid-like density is adsorbed on the solid. For a complete wetting situation, with $\theta = 0$, very thick liquid-like films intrude between the bulk gas and the solid as $\Delta\mu \to 0$. Such wetting films also play an important role in capillary condensation. For large H and small $\Delta\mu$, the density profile of the gas configuration in the slit has the form shown in Fig. 4(a). Near $z = t$ and $z = H - t$, where t is the thickness of a single wetting film, the profile resembles that of a free liquid–gas interface. Thus we might argue that a sensible approximation for the grand potential should be

$$\Omega_g \approx -pV_g - p_l^+ V_l + \gamma_{sl} A_{sl} + \gamma_{lg} A_{lg},$$

where V_g is the volume occupied by gas, V_l the volume occupied by the wetting film of metastable liquid, and A_{lg} is the area of the liquid–gas interface. The profile of the liquid configuration is sketched in Fig. 4(b). This has an approximate grand potential given by Eq. (2) with $V = V_g + V_l$ and $A_{sf} = A_{sl}$. Condensation will occur when

$$p - p_l^+ = \gamma_{lg} A_{lg}/V_g = 2\gamma_{lg}/(H - 2t). \tag{6}$$

The right-hand side is the Laplace expression for the pressure difference across a cylindrical meniscus whose mean radius of curvature[27] is $(H - 2t)$; in the limit $H \gg t$ Eq. (6) reduces to the macroscopic limit Eq. (4). It is important to note that Eq. (6) is inapplicable for models in which the solid–fluid attractive potential exhibits algebraic decay with z.[5,6] If this potential decays as $-z^{-m}(m > 2)$, for large z, the denominator must be replaced by $H - 2t_0 - 2t_0/(m-1)$, where t_0 is the equilibrium film thickness as determined from a self-consistent minimization of Ω_g. For nonretarded van der Waals (dispersion) forces, $m = 3$ and $H - 2t$ is replaced by $H - 3t_0$. Only for exponentially decaying or finite-ranged potentials is Eq. (6) recovered from a microscopic treatment of thick films.[6]

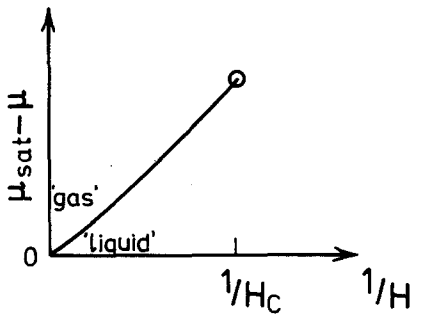

FIG. 5. A possible first-order transition line for a fluid in a capillary at a fixed temperature. The slope of this line near the origin is $2\gamma_{lg}\cos\theta/(\rho_l-\rho_g)$ [see Eq. (5)]. The line is assumed to end at a capillary critical point at a wall separation H_c and chemical potential μ_c.

The form of Eq. (5) suggests the construction of a capillary phase diagram using $\Delta\mu$ and $1/H$ as variables. For a given temperature, capillary coexistence between liquid and gas configurations is denoted by a line in the $(\Delta\mu, 1/H)$ plane (see Fig. 5). This line has a limiting slope $2\gamma_{lg}\cos\theta/(\rho_l-\rho_g)$ as $H\to\infty$. The continuation of the line to larger $\Delta\mu$ and $1/H$ is not immediate. It is tempting to speculate that $1/H$ plays a role analogous to that of temperature in determining the bulk vapor pressure $p_{sat}(T)$ [or $\mu_{sat}(T)$] curve. Then one might argue that for sufficiently large $1/H$ and $\Delta\mu$ the line of capillary coexistence should end in a capillary critical point beyond which there is only one fluid configuration in the slit. Such a possibility is indicated in Fig. 5. The analogy is made clearer by introducing an appropriate order parameter to characterize the phase transition. An obvious choice employs the difference $\Delta\rho^M \equiv \rho_l^M - \rho_g^M$ between the midpoint densities $\rho^M \equiv \rho(H/2)$ of distinct liquid and gas configurations.[28] In Fig. 6 we sketch a possible capillary coexistence curve, for fixed T, in the $(1/H, \rho^M)$ plane. This should be compared with a bulk coexistence curve in the (T,ρ) plane. At a capillary critical point $H=H_c$, $\Delta\rho^M$, vanishes. At $H=\infty$, we recover bulk coexistence $\Delta\mu=0$, and $\rho_g^M=\rho_g$ and $\rho_l^M=\rho_l$, the bulk coexisting densities. The other coexisting states in Fig. 6 correspond to $\Delta\mu>0$.

There are, of course, other possible choices of variables for illustrating capillary coexistence and critical points. For example, Nakanishi and Fisher,[17] in a study of closely related problems, chose to fix the separation H and vary the temperature rather than construct isotherms. The choice of variables is sometimes dictated by the experimental situation under investigation, but is often a matter of taste.

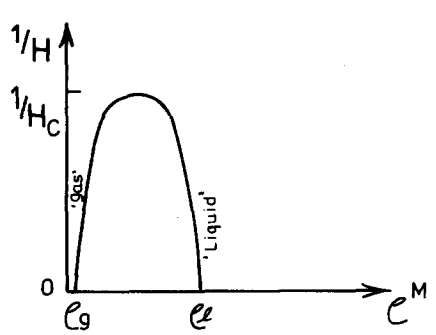

FIG. 6. Schematic capillary coexistence curve for a fixed temperature. The midpoint densities ρ_g^M and ρ_l^M of coexisting configurations are plotted for different wall separations H.

That there should be a critical point in a diagram such as Fig. 5 is not immediately evident. The argument presented above is based on a somewhat tenuous analogy with the bulk. As T increases in the bulk fluid the effects of attractive forces between the molecules are reduced and eventually these become insufficient to produce two distinct phases leaving only a single symmetric fluid state for $T>T_c$. In the capillary increasing $1/H$ allows the effects of the attractive external (solid–fluid) forces to become progressively stronger; these tend to increase the effective chemical potential. The reduction in H also reduces the net amount of fluid–fluid attraction and the combined effect is the disappearance of the two-phase coexistence when H is reduced to H_c. "Criticality" now means that two hitherto distinct fluid configurations, characterized by distinct density profiles, but with the same grand potential become indistinguishable. One of the aims of this paper is to elucidate the factors which bring about critical points in capillaries and to determine their location. We do not, however, place emphasis on small "shifts" of the bulk critical temperature arising from finite size and wall effects as this subject already has a large literature.[17] We emphasize rather the first order transition, with its accompanying capillary coexistence, and the critical points that occur at temperatures well below T_c.

III. THEORY

In order to obtain detailed information concerning capillary coexistence and critical points a quantitative or semiquantitative theory of the inhomogeneous fluid confined in the capillary is required. The theory must be able to account for wetting films and provide a realistic description of bulk coexistence. We have developed a suitable theory by generalizing the approach used by Sullivan[24,25] in his elegant mean-field treatment of adsorption, wetting transitions, and contact angles at a single wall.

A. Equation for the density profile

We consider a model intrinsic Helmholtz free energy functional

$$\mathcal{F}[\rho] = \int d\mathbf{r}\, f_h(\rho(\mathbf{r})) + \tfrac{1}{2}\int\int d\mathbf{r}\, d\mathbf{r}'\, \rho(\mathbf{r})\rho(\mathbf{r}')w_2(|\mathbf{r}-\mathbf{r}'|). \tag{7a}$$

The free energy arising from repulsive interactions between fluid molecules is treated in local density approximation: $f_h(\rho)$ is the Helmholtz free energy density of a uniform hard-sphere fluid of density ρ. Attractive forces are treated in mean-field fashion—$w_2(r)$ is the attractive part of the pairwise potential between two fluid molecules. It is well known that functionals of this type omit short-ranged correlations arising from excluded volume effects so that the resulting density profiles $\rho(\mathbf{r})$ do not exhibit the oscillations which occur for fluids near repulsive walls.[24,25] We return to this defect of the theory at a later stage. The equilibrium profile is

obtained by minimizing the grand potential functional[29]

$$\Omega_V[\rho] = \mathcal{F}[\rho] - \int d\mathbf{r}(\mu - V(\mathbf{r}))\rho(\mathbf{r}), \tag{7b}$$

where $V(\mathbf{r})$ is the total solid–fluid potential, i.e., $\rho(\mathbf{r})$ satisfies

$$\mu = V(\mathbf{r}) + \mu_h(\rho(\mathbf{r})) + \int d\mathbf{r}'\,\rho(\mathbf{r}')w_2(|\mathbf{r}-\mathbf{r}'|) \tag{8}$$

with $\mu_h(\rho) = d\mathcal{f}_h/d\rho$ the hard-sphere chemical potential. $\mu_h(\rho)$ is a monotonically increasing function of ρ. For special choices of $w_2(r)$ and $V(\mathbf{r})$, Eq. (8) can be transformed into a nonlinear differential equation. Following Sullivan[24] we set

$$w_2(r) = -\alpha\lambda^3 e^{-\lambda r}/4\pi\lambda r \tag{9a}$$

and the solid–fluid potential due to a single wall

$$V_s(\mathbf{r}) \equiv V_s(z) = \begin{cases} \infty & z<0 \\ -\epsilon_w e^{-\lambda z} & z>0. \end{cases} \tag{9b}$$

The parameters α and ϵ_w are positive; they are measures of the strength of the attractive fluid–fluid and solid–fluid potentials, respectively. λ^{-1} is the decay length of *both* potentials. The total solid–fluid potential for the slit-like capillary is

$$V(\mathbf{r}) \equiv V(z) = V_s(z) + V_s(H-z) = \begin{cases} \infty & z<0 \\ -\epsilon_w(e^{-\lambda z} + e^{-\lambda(H-z)}) & 0<z<H \\ \infty & z>H. \end{cases} \tag{10}$$

From Eqs. (8) and (9a) it follows that the profile $\rho(z)$ satisfies

$$\mu = \mu_h(\rho(x)) + V(x) - \frac{\alpha}{2}\int_0^{\lambda H} dx'\,\rho(x')e^{-|x-x'|} \tag{11}$$

with $x \equiv \lambda z$, a dimensionless length. Differentiating Eq. (11) twice with respect to x, and using the fact that $d^2V(x)/dx^2 = V(x)$ for $0<x<\lambda H$, we find that the profile obeys

$$\frac{d^2\mu_h(\rho(x))}{dx^2} = \mu_h(\rho(x)) - \mu - \alpha\rho(x). \tag{12}$$

While this equation is identical to that derived by Sullivan[24] for a single wall, the boundary conditions are different. In the present case symmetry dictates that $d\rho/dx = 0$ at $x = \lambda H/2$, whereas in the single wall problem both $d\rho/dx$ and $d^2\rho/dx^2$ vanish as $x \to \infty$, i.e., in the bulk fluid. Nevertheless, it is convenient to consider the function $\psi(\mu_h)$ introduced by Sullivan

$$\psi(\mu_h) = (\mu_h - \mu)^2 - 2\alpha(p_h - p), \tag{13}$$

where $p_h \equiv p_h(\rho(x))$ is the local hard-sphere pressure and p is the pressure of the reservoir. Using the relation $(\partial p_h/\partial\mu_h) = \rho$ it follows that Eq. (12) is equivalent to

$$\left(\frac{d\mu_h}{dx}\right)^2 = \psi(\mu_h) - \Delta p, \tag{14}$$

where Δp is a constant, independent of x, whose value depends on μ, T, and H. In the limit $H \to \infty$, $\Delta p(H) \to 0$ and Eq. (14) reduces to the single-wall result.[24] In this case there is bulk fluid in the center of the slit with density ρ_b. Since the pressure and chemical potential are given by

$$p = p_h(\rho_b) - \alpha\rho_b^2/2 \tag{15a}$$

and

$$\mu = \mu_h(\rho_b) - \alpha\rho_b, \tag{15b}$$

respectively, $\psi(\mu_h(\rho_b)) = 0$. But $d\mu_h/dx \to 0$ as $x \to \infty$ so Eq. (14) implies $\Delta p = 0$ in this limit. Δp takes on nonzero values for finite H. The function $\Delta p(H)$ may be determined from

$$\frac{\lambda H}{2} = \int_{\mu_h^w}^{\mu_h^M} d\mu_h \frac{1}{\pm(\psi(\mu_h) - \Delta p)^{1/2}} \tag{16}$$

and

$$\psi(\mu_h^M) - \Delta p = 0, \tag{17}$$

both of which follow from Eq. (14), together with Eq. (19) given below. $\mu_h^M \equiv \mu_h(\rho^M)$ is the hard sphere chemical potential at the midpoint density $\rho^M = \rho(\lambda H/2)$ and μ_h^w is the corresponding quantity at the wall $\mu_h^w \equiv \mu_h(\rho(0)) = \mu_h(\rho(\lambda H))$. The choice of sign is Eq. (16) depends on whether μ_h or, equivalently, $\rho(x)$, is a monotonically increasing or decreasing function of x in the range $0<x<\lambda H/2$. This depends, in turn, on the boundary conditions at both $x=0$ and $x=\lambda H/2$. The "wall" boundary condition is obtained by differentiating Eq. (11) with respect to x and using Eq. (10),

$$\left(\frac{d\mu_h}{dx}\right)_{x=0} = \mu_h^w - \mu - 2\epsilon_w = -\left(\frac{d\mu_h}{dx}\right)_{x=\lambda H}. \tag{18}$$

This is identical to the single wall condition.[24] It may be reexpressed as

$$\psi(\mu_h^w) - \Delta p = (\mu_h^w - \mu - 2\epsilon_w)^2. \tag{19}$$

Once $\Delta p(H)$ is determined, $\mu_h(x)$, and hence $\rho(x)$, can be obtained by integrating Eq. (14). Later we shall see that the grand potential for a given configuration can be expressed simply in terms of $\Delta p(H)$.

B. Graphical construction for $\Delta p(H)$

The function $\psi(\mu_h)$ has its extrema where $\mu_h = \mu + \alpha\rho(\mu_h)$. It takes its minimum value of zero at $\mu_h^b \equiv \mu_h(\rho_b)$. A second minimum $\psi^+ > 0$ occurs at $\mu_h^+ > \mu_h^b$, provided $\mu > \mu_{\min}$ in Fig. 3, so that the equation $\mu = \mu(\rho) = \mu_h(\rho) - \alpha\rho$ still has three roots. μ_h^+ refers to the metastable liquid at chemical potential μ. From Eq. (13),

$$\psi^+ = \psi(\mu_h^+) = \alpha^2\rho^{+2} - 2\alpha(p_h^+ - p)$$

which can be written as

$$\psi^+ = 2\alpha(p - p_l^+), \tag{20}$$

where $p_l^+ = p_h^+ - \alpha\rho^{+2}/2$ is the pressure of the metastable liquid of density ρ^+. In the limit $\Delta\mu \to 0$, $\rho_b \to \rho_g$, the second minimum deepens $\psi^+ \to 0$ and $\mu_h^+ \to \mu_h^l$, the hard-sphere chemical potential appropriate to the coexisting liquid of density ρ_l. A sketch of $\psi(\mu_h)$ is given in Fig. 7(a) along with the parabola $I(\mu_h) = (\mu_h - \mu - 2\epsilon_w)^2$. The difference between these functions $\psi - I$ is also plotted. We denote this Δp^w [see Eq. (19)]. Δp^w has its maximum at $\mu_h(\rho)$ with $\rho = 2\epsilon_w/\alpha$. On the other hand, Eq. (17) implies $\Delta p = \psi(\mu_h^M) > 0$. The nature of the graphical construction for $\Delta p(H)$, or more accurately $H(\Delta p)$, is apparent now. Set $\Delta p = c$, a constant. Choose $c > 0$, but $<$ the maximum of

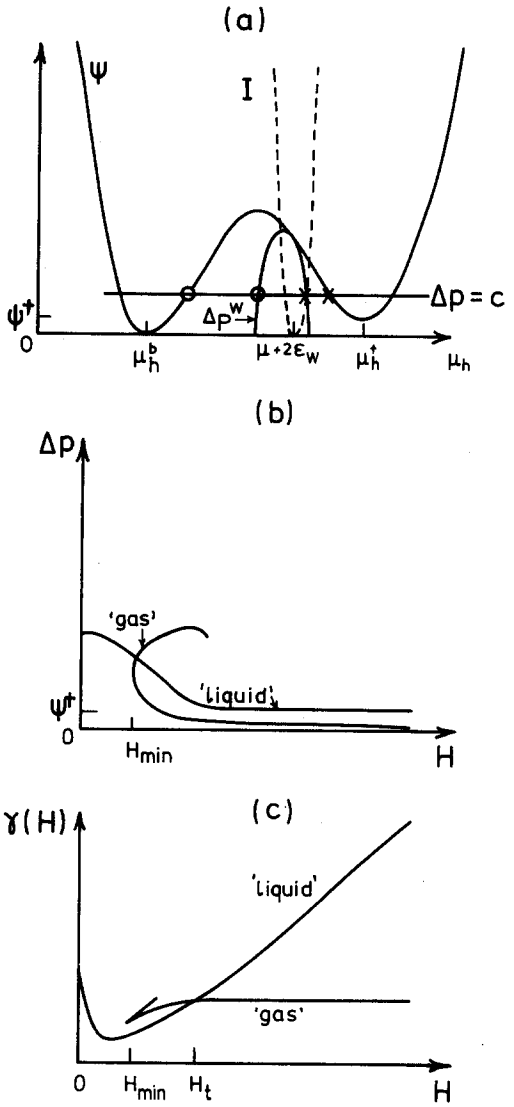

FIG. 7. (a) Sketch of the functions $\psi(\mu_h)$, $I(\mu_h)$, and $\Delta p^w = \psi - I$ for a partial wetting situation and a small undersaturation $\Delta\mu$. Δp^w meets ψ tangentially at hard sphere chemical potential $\mu_h = \mu + 2\epsilon_w$, the minimum of $I(\mu_h)$. The circles correspond to midpoint value μ_h^M and wall value μ_h^w for a gas configuration while the crosses correspond to μ_h^w and μ_h^M for a liquid configuration with $\Delta p = c$, a constant (see the text). (b) Sketch of $\Delta p(H)$ as obtained from (a) Both liquid and gas branches extend to $H = \infty$, but only liquid extends to $H = 0$. (c) Sketch of the interfacial free energy $\gamma(H)$ as obtained from (b). $\gamma(H)$ increases linearly with H as $H \to \infty$ on the liquid branch. The gas is the stable configuration for separations $H > H_t$, whereas liquid is stable for $H < H_t$.

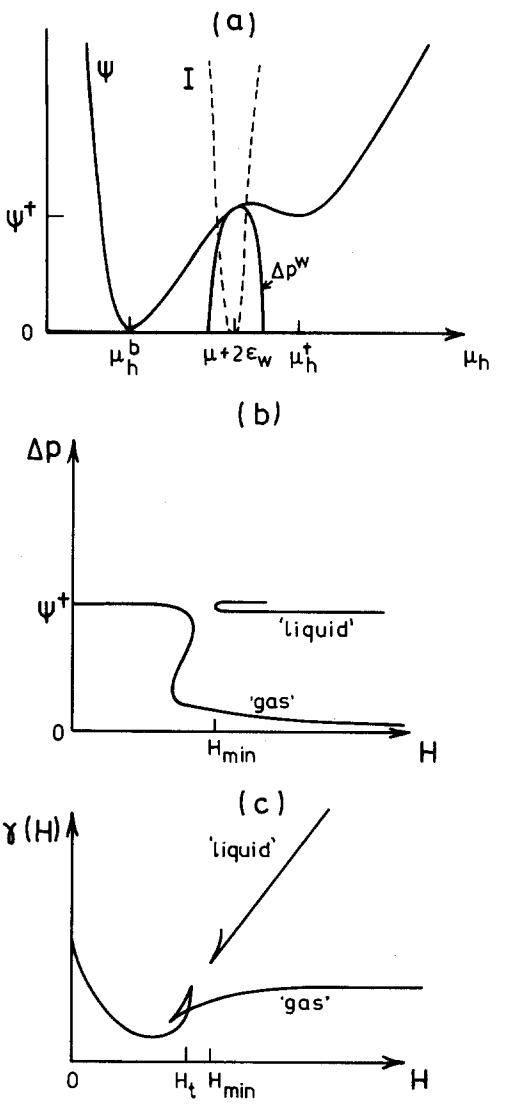

FIG. 8. (a) The same as in Fig. 7(a), but for a large undersaturation $\Delta\mu$; the minimum ψ^+ is much higher than in Fig. 7(a). (b) Sketch of $\Delta p(H)$ obtained from (a). The gas configuration now extends to $H = 0$ and exhibits a loop. Spinodals occur where $(\partial H/\partial \Delta p) = 0$. (c) Sketch of $\gamma(H)$ obtained from (b). Liquid is never stable but two distinct gas configurations corresponding to different values of Δp, coexist at $H = H_t$.

Δp^w. The intersections of the horizontal line $\Delta p = c$ with the curves ψ and Δp^w determine μ_h^M and μ_h^w, respectively. This is indicated in Fig. 7(a). Performing the integration in Eq. (16) then yields a value for H.

It is evident that there are several possible intersections for a given Δp. In Fig. 7(a), we have marked with circles the intersections that correspond to a gas like configuration; μ_h^M is small, as is appropriate to a dilute gas in the center of the slit $\mu_h^w > \mu_h^M$, $d\mu_h/dx$ and, hence, $d\rho/dx$ are negative for $0 < x < \lambda H/2$ and the minus sign must be taken in Eq. (16). A liquid configuration occurs if we consider the intersections marked by crosses. In this case both μ_h^w and μ_h^M are large, consistent with a dense liquid state. However, $\mu_h^w < \mu_h^M$ and $d\mu_h/dx$ is positive for $0 < x < \lambda H/2$, requiring the positive sign in Eq. (16). Not all integration paths are allowed; the choice is restricted by Eq. (18) and the requirement that $\mu_h(x)$ be a monotonic function for $0 < x < \lambda H/2$. It can be shown that the vanishing of the denominator of Eq. (16) at the upper limit μ_h^M does not cause the integral to become singular unless $d\psi/d\mu_h$ is zero at this point. This implies $H \to \infty$ for the gas configuration if and only if $\Delta p \to 0$. In this limit we recover the single wall solution. For the liquid configuration $H \to \infty$ if and only if $\Delta p \to \psi^+$ from above. When Δp is chosen so that $\mu_h^M \to \mu_h^w$, i.e., to coincide with the point where the curves Δp^w and ψ touch $H \to 0$. [These curves meet tangentially when $\mu_h = \mu + 2\epsilon_w$, the position of the minimum of $I(\mu_h)$.] This situation corresponds to a limiting liquid configuration in Fig. 7(a). By varying Δp and calculating H it is possible to obtain the curves for $\Delta p(H)$ sketched in

Fig. 7(b). The liquid branch exists for all values of H while the gas branch only exists for $H > H_{\min}$. If two, or more, branches exist at a given value of H the one with the lower grand potential is the stable one [see Fig. 7(c)].

These results refer to fixed μ and T and to given potential functions. If we keep T fixed but reduce μ (increase the undersaturation), we move to the situation described by Fig. 8(a). Here the minimum at μ_h^+ is much less pronounced and ψ^+ is much larger. The gas branch of $\Delta p(H)$ exists for all H whereas the liquid only exists for $H > H_{\min}$ [see Fig. 8(b)]. On reducing μ further $H_{\min}$ increases for the liquid branch. $\Delta p(H)$ exhibits a "loop" for the gas configuration. Although the size of this is exaggerated in the sketch, its presence shows that distinct gas solutions, both with $d\rho/dx$ negative for $0 < x < \lambda H/2$, but corresponding to different values of Δp, can exist for the same value of H. We return to the importance of such loops in Sec. III D.

When $\mu < \mu_{\min}$ in Fig. 3 so that $\mu = \mu_h(\rho) - \alpha\rho$ has only one root, the minimum at μ_h^+ disappears and no liquid branch exists.

It is clear that an interesting "cross-over" behavior must occur for some value μ intermediate between those appropriate to Figs. 7 and 8. When μ is such that Δp^w has its maximum precisely at the maximum of ψ the liquid branch and the uppermost gas branch of $\Delta p(H)$ meet contiguously at a certain cross-over value H_{co}. This occurs[30] when $\mu = \mu_h(\tilde{\rho}) - \alpha\tilde{\rho}$ with $\tilde{\rho} = 2\epsilon_w/\alpha$. Such behavior does not correspond to a critical point. There is another gas state, on another part of the loop in $\Delta p(H)$, with a lower grand potential that is the stable solution.

The examples described so far correspond to partial wetting situations. In the limit $H \to \infty$, the gas configurations do not exhibit thick wetting films at the walls. Such films will only develop when the minimum of $I(\mu_h)$, at $\mu_h = \mu + 2\epsilon_w$, is larger than μ_h^+. This case is illustrated in Fig. 9. Gas configurations occur for $\Delta p < \psi^+$. As is usual $H \to \infty$ as $\Delta p \to 0$, but now H also diverges in the limit $\Delta p \to \psi^+$ from below since the integration path in Eq. (16) then approaches the minimum at μ_h^+. For sufficiently small undersaturations (small ψ^+) wetting films occur on both the upper and lower gas branches of $\Delta p(H)$ in Fig. 9(b); both solutions have $\mu_h^w > \mu_h^M$ and $d\mu_h/dx$ negative. The wetting films can be identified by Taylor expanding the denominator in Eq. (16) about both minima of ψ. Near the minimum corresponding to bulk gas

$$\psi(\mu_h) = a_g^2(\mu_h - \mu_h^b)^2 + \cdots$$

and

$$\Delta p = \psi(\mu_h^M) = a_g^2(\mu_h^M - \mu_h^b)^2 + \cdots,$$

where $a_g^2 = \frac{1}{2}(d^2\psi/d\mu_h^2)_{\mu_h = \mu_h^b}$, while near the minimum corresponding to the metastable bulk liquid

$$\psi(\mu_h) = \psi^+ + a_l^2(\mu_h - \mu_h^+)^2 + \cdots$$

with $a_l^2 = \frac{1}{2}(d^2\psi/d\mu_h^2)_{\mu_h = \mu_h^+}$. Dividing up the range of the integral in Eq. (16) into appropriate intervals and performing the integration we find that in the limits $\psi^+ \to 0$, $\Delta p \to 0$,

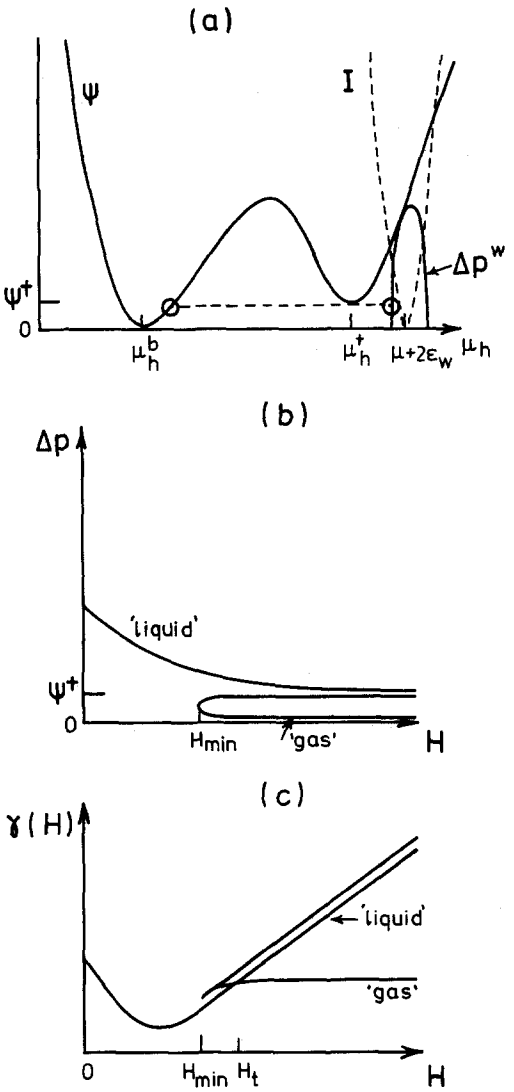

FIG. 9. (a) The same as Fig. 7(a) but for a complete wetting situation so that $\mu + 2\epsilon_w > \mu_h^+$. The horizontal dashed line corresponds to $\Delta p \lesssim \psi^+$ and the circles mark its intersections with ψ and Δp^w, i.e., μ_h^M and μ_h^w. The corresponding density profile exhibits thick wetting films. (b) $\Delta p(H)$ obtained from (a). The upper gas and liquid branches both approach ψ^+ as $H \to \infty$. As $\Delta\mu$ is reduced, ψ^+ is lowered and $H_{\min}$ increased. (c) $\gamma(H)$ obtained from (b). Both the liquid and upper gas branches have constant slope $\psi^+/4\alpha$ as $H \to \infty$. A first order transition from gas to liquid occurs as H is reduced to H_t.

and $H \to \infty$:

$$\frac{\lambda H}{2} \approx -\frac{1}{a_g}\ln\left(\frac{\Delta p(H)}{a_g^2\Theta^2}\right)^{1/2} - \frac{1}{a_l}\ln\left(\frac{\psi^+ - \Delta p(H)}{4a_l^2\Theta^2}\right), \tag{21}$$

where Θ is a constant. The first term is associated with the bulk gas; it is not specific to the wetting situation but indicates that Δp decreases exponentially with increasing H on the lower gas branch in Fig. 9(b). The second term is associated with the metastable liquid at $\mu_h = \mu_h^+$. It is of precisely the same form as the quantity[31] that determines the thickness of a wetting film at a single wall, except that ψ^+ is now replaced by $\psi^+ - \Delta p(H)$. Thus the film thickness in the slit

$t(H)$ is given, approximately, by

$$\lambda t(H) \approx -\frac{1}{a_l} \ln\left(\frac{\psi^+ - \Delta p(H)}{4a_l^2 \Theta^2} \right). \tag{22}$$

In the limit $\Delta p \to 0, H \to \infty$ and $t(H) \to t(\infty)$, the thickness at a single wall. For finite $H, \Delta p(H)$ is greater than zero so $t(H) > t(\infty)$ for a given ψ^+. That wetting films should be thicker, for a given undersaturation, in capillaries than at a single wall follows from general considerations.[6,12] On the lower gas branch $d\Delta p/dH$ is negative so the film thickness increases as H is reduced towards $H_{\min}$. On the upper gas branch, which corresponds to an unstable solution, $t(H)$ increases as $H \to \infty$ in such a manner that H-$2t(H)$ remains roughly constant. This follows by rewriting Eq. (21) as

$$\lambda\,[H - 2t(H)] \approx -\frac{2}{a_g} \ln\left(\frac{\Delta p(H)}{a_g^2 \Theta^2} \right)^{1/2} \tag{23}$$

and recognizing that as $H \to \infty$ on this branch $\Delta p \to \psi^+$, a constant. For $H < H_{\min}$, no gas configuration exists; a similar result was obtained earlier by Derjaguin and Churaev[12] based on a model for the disjoining pressure. Note that as $\psi^+ \to 0, H_{\min} \to \infty$. We shall see that this has repercussions for the form of adsorption isotherms.

A separate liquid configuration exists for $\Delta p > \psi^+$. Unlike the partial wetting case $\mu_h^w > \mu_h^M$ and $d\mu_h/dx$ is negative now. The branch exists for all H and $H \to \infty$ as $\Delta p \to \psi^+$ from above—provided ψ exhibits the second minimum at μ_h^+. If the undersaturation is increased sufficiently so that $\mu < \mu_{\min}$ in Fig. 3 there is no metastable bulk liquid at that value of μ. In these circumstances (see Fig. 10), the upper gas branch does not extend to $H = \infty$, but reverses direction at $H = H_{\max}$ and continues to $H = 0$. Thus the loop in $\Delta p(H)$ becomes closed. The uppermost branch which extends to $H = 0$, could be regarded as liquid as μ_h^w and μ_h^M take on large values, but it is important to recognize that this no longer extends to $H = \infty$.

Finally, we remark that it is also possible to consider situations for which $\mu + 2\epsilon_w < \mu_h^b$. No liquid configurations exist now but the gas exists for all values of H.

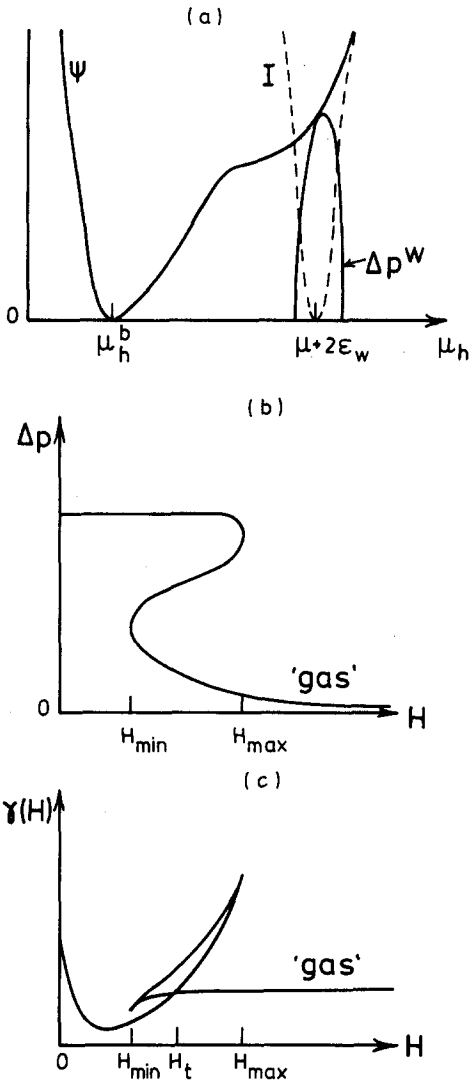

FIG. 10. (a) The same as in Fig. 7(a), but for a case where the fluid is strongly undersaturated so that ψ has no second minimum (no metastable bulk liquid). (b) $\Delta p(H)$ obtained from (a). Spinodal points occur at $H_{\min}$ and $H_{\max}$. If $\Delta\mu$ is increased further the loop shrinks. (c) $\gamma(H)$ obtained from (b). Cusps occur at the spinodal points. Two distinct fluid configurations coexist at $H = H_t$. The loop in $\gamma(H)$ shrinks on increasing $\Delta\mu$ and disappears at the capillary critical point.

C. The interfacial free energy on different branches of $\Delta p(H)$

The interfacial free energy $\gamma(H)$ can be expressed rather simply for the present model system. From Eqs. (1) and (7) we have

$$2\gamma(H) = \int_0^H dz \left\{ p + f_h(\rho(z)) + \tfrac{1}{2}\rho(z) \int d\mathbf{r}' \rho(z') w_2(|\mathbf{r} - \mathbf{r}'|) + \rho(z)(V(z) - \mu) \right\}.$$

Using Eq. (11) and following the procedure employed by Sullivan[25] for a single wall this can be reduced to

$$2\gamma(H) = H\Delta p(H)/2\alpha + \frac{1}{\alpha\lambda} \left[(\mu_h^w - \mu - 2\epsilon_w)^2 - 2\epsilon_w^2 (1 - e^{-\lambda H}) \pm 2 \int_{\mu_h^w}^{\mu_h^M} d\mu_h (\psi(\mu_h) - \Delta p(H))^{1/2} \right], \tag{24}$$

where the choice of sign outside the integral is determined by the same considerations as previously. In the limit $\Delta p \to 0$, $H \to \infty$ and Eq. (24) reduces to Sullivan's formula[25] for $\gamma(\infty)$, the surface tension of the solid–fluid interface at a single wall. For a configuration to remain stable as $H \to \infty$, $\Delta p(H)$ must vanish exponentially. For finite H, however, it is necessary to evaluate Eq. (24) for the various possible branches of $\Delta p(H)$ to determine the stable solution, i.e., the one with the lowest $\gamma(H)$.

The derivative $(\partial\gamma/\partial H)_{\mu,T}$ is related directly to $\Delta p(H)$. Differentiating Eq. (24) with respect to Δp, we obtain

$$2\frac{\partial\gamma}{\partial\Delta p}=\frac{1}{2\alpha}\left(\frac{\partial H}{\partial\Delta p}\Delta p+H\right)+\frac{1}{\alpha\lambda}\left[2(\mu_h^w-\mu-2\epsilon_w)\frac{\partial\mu_h^w}{\partial\Delta p}-2\lambda\epsilon_w^2e^{-\lambda H}\frac{\partial H}{\partial\Delta p}\right.$$
$$\left.\pm 2\frac{\partial\mu_h^M}{\partial\Delta p}(\psi(\mu_h^M)-\Delta p)^{1/2}\mp 2\frac{\partial\mu_h^w}{\partial\Delta p}(\psi(\mu_h^w)-\Delta p)^{1/2}\pm 2\int_{\mu_h^w}^{\mu_h^M}d\mu_h\frac{\partial}{\partial\Delta p}(\psi(\mu_h)-\Delta p)^{1/2}\right],$$

where it is understood that μ and T are fixed. The terms in $\partial\mu_h^w/\partial\Delta p$ cancel by virtue of Eq. (19) while the term in $\partial\mu^M/\partial\Delta p$ vanishes as a result of Eq. (17). The integrand in the last term can be reexpressed as $\mp\frac{1}{2}(d\mu_h/dx)^{-1}$ by virtue of Eq. (14) so the integral reduces to $\mp\lambda H/4$. Combining terms, we find

$$2\frac{\partial\gamma}{\partial\Delta p}=\frac{1}{2\alpha}\frac{\partial H}{\partial\Delta p}(\Delta p-4\epsilon_w^2e^{-\lambda H})$$

or

$$\frac{\partial\gamma(H)}{\partial H}=\frac{1}{4\alpha}(\Delta p(H)-4\epsilon_w^2e^{-\lambda H}). \tag{25}$$

The asymptotic behavior of $\gamma(H)$ is determined by that of $\Delta p(H)$. On a stable branch we find from Eq. (21) that as $H\to\infty$:

$$\Delta p(H)\sim Ce^{-\lambda a_g H}, \tag{26}$$

where C is a constant. Since μ_h increases monotonically with ρ it follows that $a_g^2=\frac{1}{2}(d^2\psi/d\mu_h^2)_{\mu_h=\mu_h^b}=1-\alpha(d\rho/d\mu_h)_{\mu_h=\mu_h^b}$ is <1. Thus $\Delta p(H)$ decays more slowly than the other exponential term in Eq. (25) and, as it is positive, this implies $\gamma(H)\to\gamma(\infty)$ the solid gas surface tension as $H\to\infty$. On a metastable liquid branch $\Delta p\to\psi^+$ as $H\to\infty$ and Eq. (25) yields

$$\gamma_l(H)\sim\psi^+H/4\alpha+\gamma_{sl}+O(e^{-\lambda a_l H})+O(e^{-\lambda H}), \tag{27}$$

where γ_{sl} is the solid–liquid surface tension at saturation. Inserting this result into Eq. (1), ignoring exponential terms and using Eq. (20) for ψ^+, we recover the macroscopic expression (2) for the grand potential of a liquid configuration in a wide capillary.

Using Eq. (24) or Eq. (25), we can construct $\gamma(H)$. In Figs. 7–10 we sketch this function for the four examples discussed in the previous section. $\gamma(H)$ for the gas configuration in Fig. 7(c) exhibits a cusp at $H=H_{min}$ where $\partial\Delta p/\partial H$ diverges. The gas has the lower interfacial free energy for $H>H_t$, but the liquid becomes the stable configuration for $H<H_t$. Since $\partial\gamma/\partial H$ is discontinuous at $H=H_t$ a first order transition occurs at this separation. This transition corresponds to condensation from the gas shown in Fig. 2(a) to the liquid configuration sketched in Fig. 2(b). It arises from the mechanism described in Sec. II. As $\Delta\mu$ is reduced, so that ψ^+ decreases, H_t is shifted to large values and the macroscopic formula (4) becomes rather accurate. For larger $\Delta\mu$, however, the macroscopic argument fails. This becomes clear in Fig. 8(c). Here the liquid branch is not the stable branch for any value of H, so the picture of the metastable liquid becoming the stable configuration at small H is no longer appropriate. The liquid branch is removed from the gas branch which now exhibits a loop with two cusps corresponding to two singularities of $\partial\Delta p/\partial H$ in Fig. 8(b). At the value of H where the loop in $\gamma(H)$ closes, two distinct gas configurations have the same grand potential, i.e., they coexist in the capillary.

For some intermediate value of $\Delta\mu$ the cross-over situation described earlier will occur. The cusp in the liquid branch of $\gamma(H)$ at H_{min} then touches the upper cusp in the gas branch. However, the stable solution at that value of H is on the lower gas branch (as stated previously).

Figure 9(c) shows $\gamma(H)$ for a complete wetting situation. For large H, the lower gas branch of $\Delta p(H)$ is stable and $\gamma(H)\to\gamma(\infty)$ as $H\to\infty$. Since $\Delta p(H)\to\psi^+$ as $H\to\infty$ on the upper gas branch, $\gamma(H)$ has a positive slope, equal to $\psi^+/4\alpha$ at large H. The liquid branch has the same slope but corresponds to a lower free energy. Thus the liquid can be regarded as metastable at large H. It becomes the stable configuration for $H<H_t$. The two configurations that coexist at $H=H_t$ have density profiles of the type shown in Fig. 4.

For small ψ^+ it is possible to recover the approximate result of Eq. (6). This is achieved most easily by considering the surface tension in the limit $H=\infty$, where $\Delta p=0$. The main effect of a small undersaturation is to raise the minimum of ψ at μ_h^+ from zero to ψ^+. If we assume μ_h^w and μ_h^M remain unchanged and we Taylor expand ψ near μ_h^+, we find from Eq. (24) that

$$\gamma(\infty)\approx\gamma_{sg}+\frac{1}{\alpha\lambda}\int_{\mu_h^+-\Theta}^{\mu_h^++\Theta}$$
$$\times d\mu_h\left[(\psi^++a_l^2(\mu_h-\mu_h^+)^2)^{1/2}-a_l(\mu_h-\mu_h^+)\right],$$

where γ_{sg} is $\gamma(\infty)$ evaluated at saturation ($\Delta\mu=0$) and Θ is a constant. The second integral is zero and the first can be transformed to

$$\int_{-\Theta}^{\Theta}dy(\psi^++a_l^2y^2)^{1/2}$$
$$=\Theta(\psi^++a_l^2\Theta^2)^{1/2}+\frac{\psi^+}{2}\int_{-\Theta}^{\Theta}dy(\psi^++a_l^2y^2)^{-1/2}.$$

But the last integral is identical to that which determines $t(\infty)$, the thickness of the wetting film at a single wall,[31] so we may write

$$\gamma(\infty)\approx\gamma_{sg}+\psi^+t(\infty)/2\alpha$$

which states that the interfacial tension is increased by an amount proportional to the film thickness. Integrating Eq. (25) and making use of Eq. (21) for $\Delta p(H)$ we find

$$\gamma_{\rm wet}(H)\sim\gamma_{sg}+\psi^+t(H)/2\alpha$$
$$+O(e^{-\lambda(H-2t(H))})+O(e^{-\lambda H}) \tag{28}$$

for a gas configuration with wetting films. Condensation will take place to the liquid when $\gamma_{\rm wet}(H_t)=\gamma_l(H_t)$. Ignoring ex-

ponential contributions this requires

$$\gamma_{sg} - \gamma_{sl} = \gamma_{lg} = \psi^{+}(H_t - 2t(H_t))/4\alpha.$$

Using Eq. (3) and (20) this result reduces to Eq. (6). It can be combined with Eq. (22) to provide an approximation for the thickness of the wetting film in the gas configuration that coexists with the liquid. We find

$$\lambda t(H_t) \sim -\frac{1}{a_l} \ln(\alpha\gamma_{lg}/a_l^2\Theta^2 H_t),$$

i.e., the thickness increases logarithmically with wall separation.[32] In order that thick films may exist as the *stable* configuration it is necessary to have very wide capillaries. This has important repercussions for the observation of wetting films in pores and in computer simulation.

When the bulk fluid is at the spinodal, $\mu = \mu_{\min}$ in Fig. 3, so that the minimum of ψ at μ_h^+ becomes a point of inflection, the upper gas and "liquid" branches of $\Delta p(H)$ and $\gamma(H)$ meet at $H = \infty$. For larger undersaturations, $\gamma(H)$ takes the form shown in Fig. 10(c). A first order transition from a gas to a denser fluid configuration occurs at $H = H_t$. However, the asymptotic analysis given above is no longer applicable since there is no metastable bulk fluid and no wetting films.

It is evident that a first order transition between two distinct configurations can arise from two rather different mechanisms. The first, which occurs for small undersaturations, is equivalent to the macroscopic argument given in Sec. II and involves the condensation of the metastable bulk liquid. The second, which occurs at larger undersaturations, involves the loop in $\Delta p(H)$. We examine this second case further.

D. Loops, capillary spinodals, and the origin of critical points

When loops arise in $\Delta p(H)$ it is possible to determine the value of H for which coexistence occurs by means of a construction analogous to the Maxwell construction employed for bulk coexistence. This is illustrated in Fig. 11. From Eq. (25), we have at fixed μ and T:

$$\gamma(H) = \frac{1}{4\alpha}\int_0^H dH'(\Delta p(H') - 4\epsilon_w^2 e^{-\lambda H'}) - \gamma(0).$$

If the two configurations corresponding to Δp_α and Δp_β have equal interfacial tension $\gamma(H_t)$, at $H = H_t$ it follows that

$$\int_\alpha^\beta dH' \Delta p(H') = 0,$$

where the integral is taken along the curve between Δp_α and Δp_β. This implies that the areas in the figure satisfy $-(B+D)+(B+C+A)-A=0$, where the sign is taken to be negative if $d\Delta p/dH$ is negative on the appropriate part of the curve. Thus the areas C and D must be equal for coexistence. Note also that the portions with $d\Delta p/dH$ positive correspond to unstable portions (between the cusps) of $\gamma(H)$.

Critical points are associated with the disappearance of the loops in $\Delta p(H)$ as the undersaturation is increased. In the partial wetting situation depicted in Fig. 8, a small increase in $\Delta\mu$ rapidly decreases the areas C and D and the density profiles of the coexisting configurations become closer. At the critical point the areas vanish [see Fig. 11(b)] and the profiles are identical. Eventually, $\Delta p(H)$ becomes a monotonically decreasing function of H and there is only one solution for a given H [see Fig. 11(c)]. The same mechanism occurs for the complete wetting situation.

The important difference between the two different wetting regimes is that the loops are much larger for a complete wetting. (This also facilitates numerical work.) In the case of partial wetting the loops are already very small at the crossover situation so that the critical point lies close to the crossover point. Indeed, in our earlier paper,[26] we identified the critical point with the crossover. More accurate calculations show that the coexistence lines extend beyond those given in Ref. 26; we discuss this later.

The critical point corresponds to the conditions

$$\left(\frac{\partial H}{\partial \Delta p}\right)_{\mu,T}^{c} = \left(\frac{\partial^2 H}{\partial \Delta p^2}\right)_{\mu,T}^{c} = 0 \tag{29}$$

together with the constraint that H be given by Eq. (16). Alternatively we can require

$$\left(\frac{\partial H}{\partial \mu_h^M}\right)_{\mu,T}^{c} = \left(\frac{\partial^2 H}{\partial \mu_h^{M^2}}\right)_{\mu,T}^{c} = 0 \tag{30}$$

since plots of $\mu_h^M(H)$, the hard-sphere chemical potential at midpoint, have the same form as those of $\Delta p(H)$ shown in Fig. 11. Equation (29) or Eq. (30) determine the critical values of μ and H for a fixed T. Noting that μ_h^M can be replaced by ρ^M, the density at midpoint, in Eq. (30) the genesis of a capillary coexistence curve like that sketched in Fig. 6 becomes apparent.

Making a further analogy with the bulk fluid it is pertinent to enquire about the nature of capillary spinodals. For fixed μ and T, the spinodal midpoint densities are defined by

$$\left(\frac{\partial H}{\partial \mu_h^M}\right)_{\mu_h^M=\mu_{h,1}^M} = 0 = \left(\frac{\partial H}{\partial \mu_h^M}\right)_{\mu_h^M=\mu_{h,2}^M}. \tag{31}$$

Since $(\partial\Delta p/\partial\mu_h^M)_{\mu,T} = (\partial\psi(\mu_h^M)/\partial\mu_h^M)_{\mu,T}$ is nonzero in the

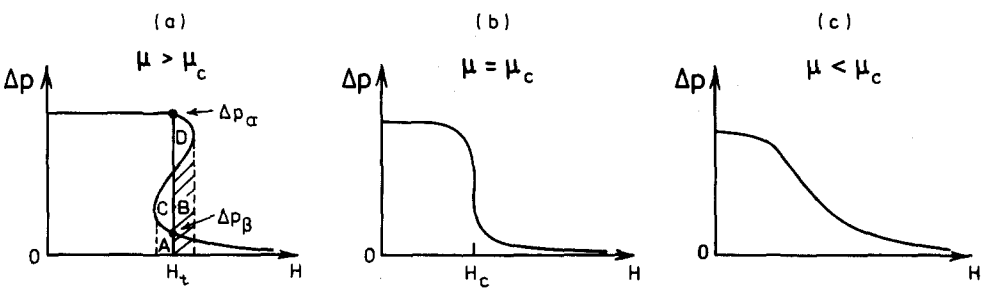

FIG. 11. Sketch of $\Delta p(H)$ for three different chemical potentials μ and fixed temperature. (a) $\mu_{sat} > \mu > \mu_c$. An equal area construction ($C = D$) yields the values of Δp_α and Δp_β of the two configurations coexisting at $H = H_t$ (see the text). (b) $\mu = \mu_c$, the critical value. (c) $\mu < \mu_c$.

range of interest Eq. (31) is equivalent to $(\partial H/\partial \Delta p)_{\mu,T}=0$. Thus the singularities in $\partial \Delta p/\partial H$ and therefore the cusps in $\gamma(H)$ correspond to spinodal points. By differentiating Eq. (16) with respect to μ_h^M and using Eq. (19) it is possible to derive an equation for the capillary spinodal points (see Appendix A). For large H (small $\Delta\mu$) closed loops in $\Delta p(H)$ no longer occur and $(\partial H/\partial \Delta p)_{\mu,T}$ exhibits only one zero, which can correspond to liquid *or* gas.

For bulk coexistence we require the pressures and chemical potentials of liquid and gas to be the same for a given T. The corresponding spinodal densities ρ_1 and ρ_2 are then given by $(\partial p/\partial \rho)_{\rho=\rho_1}=0=(\partial p/\partial \rho)_{\rho=\rho_2}$. For capillary coexistence we require $\gamma(H)$ to be the same for both phases; p and μ are fixed by the reservoir. It is natural then to seek spinodal midpoint densities from the condition

$$\left(\frac{\partial \gamma(H)}{\partial \rho^M}\right)_{\rho^M=\rho_1^M}=0=\left(\frac{\partial \gamma(H)}{\partial \rho^M}\right)_{\rho^M=\rho_2^M} \tag{32}$$

at fixed μ and T. Since $(\partial\gamma/\partial\rho^M)=(\partial\gamma/\partial H)(\partial H/\partial\mu_h^M)(\partial\mu_h^M/\partial\rho^M)$, Eqs. (31) and (32) are equivalent. The unstable portion of the bulk isotherms is that for which $(\partial p/\partial\rho)_T<0$. In the capillary the unstable portion has $(\partial H/\partial\Delta p)>0$, or alternatively, $(\partial H/\partial\mu_h^M)>0$. Moreover, as $(\partial\gamma/\partial H)$ is positive in the relevant region, it follows that $(\partial\gamma/\partial\rho^M)>0$.

It is more natural perhaps to consider derivatives with respect to μ. In Appendix B we derive expressions for $(\partial\mu_h(z)/\partial\mu)_T$ starting from Eq. (14) for the density profile. We show that this quantity diverges for $z=H/2$, when $(\partial H/\partial\mu_h^M)_{\mu,T}=0$, i.e., at a spinodal or critical point. The latter will occur when

$$\left(\frac{\partial\mu}{\partial\mu_h^M}\right)_T^c=\left(\frac{\partial^2\mu}{\partial\mu_h^{M^2}}\right)=0. \tag{33}$$

This condition,[33] which is an alternative to Eqs. (29) or Eq. (30), is now closely analogous to that employed to locate a bulk critical point; recall that μ_h^M measures the midpoint density ρ^M.

Our final analogy with the bulk involves the behavior of pairwise correlations at a critical point. In the bulk fluid the long-wavelength limit of the structure factor $S(q)$ diverges at the critical point in the same fashion as the isothermal compressibility κ_T. This follows from the relation

$$\lim_{q\to 0} S(q)=\frac{k_BT}{\rho}\left(\frac{\partial\rho}{\partial\mu}\right)_T=\rho k_BT\kappa_T \tag{34}$$

with $S(q)=1+\rho\int d\mathbf{r}\, e^{i\mathbf{q}\cdot\mathbf{r}}h(r)$. The total pair correlation function $h(r)$ becomes long ranged at the critical point. What is the analog of this behavior for a fluid at a capillary critical point? Since the fluid is inhomogeneous $h(r)$ must be replaced by $h(\mathbf{r},\mathbf{r}')\equiv h(z,z',R)$ with $R=[(x'-x)^2+(y'-y)^2]^{1/2}$, the mutual separation of particles measured parallel to the walls. It is convenient to define a transverse structure factor $S(z,Q)$ via

$$S(z,Q)\equiv 1+\int dz'\rho(z')\int d\mathbf{R}e^{i\mathbf{Q}\cdot\mathbf{R}}h(z,z',R), \tag{35}$$

where Q is a two-dimensional wave vector parallel to the walls. The $Q=0$ limit of this function is given by[34]

$$\lim_{Q\to 0} S(z,Q)=\frac{k_BT}{\rho(z)}\left(\frac{\partial\rho(z)}{\partial\mu}\right)_T, \tag{36}$$

where the derivative is performed with fixed external potential and temperature. The close similarity between Eqs. (34) and (36) allows us to treat $S(z,0)$ as being proportional to a local compressibility or susceptibility. At the capillary critical point the local compressibility at midpoint $(\partial\rho^M/\partial\mu)_T$ diverges and we expect $(\partial\rho(z)/\partial\mu)_T$ to be singular for other values of z. Such behavior will be accompanied by the growth of long-ranged transverse correlations in $h(z,z',R)$. While the precise nature of these transverse correlations and their variation with z remains to be investigated, it is clear from Appendix B that such correlations afford a signature of the approach to capillary criticality and are associated with the vanishing of the order parameter $\Delta\rho^M$. This divergence of the local compressibility is *not* associated with the capillary wave-like fluctuations that give rise to the divergence of $S(z,0)$ at the edge of a wetting film in the approach to complete wetting.[23,31] The latter divergence can only occur for an infinite system ($H=\infty$) (see Appendix B).

E. Adsorption and the force between walls

The total adsorption Γ (or coverage) in the capillary is conveniently defined by

$$\Gamma(H)=\int_0^H dz(\rho(z)-\rho_b) \tag{37}$$

with ρ_b the density of bulk fluid at chemical potential μ and temperature T. In the limit $H\to\infty$ $\Gamma(H)\to 2\Gamma_{sf}$, where Γ_{sf} is the adsorption at a single wall. $\Gamma(H)$ is related to the interfacial free energy $\gamma(H)$ via the Gibbs adsorption equation

$$\Gamma(H)=-2(\partial\gamma(H)/\partial\mu)_T. \tag{38}$$

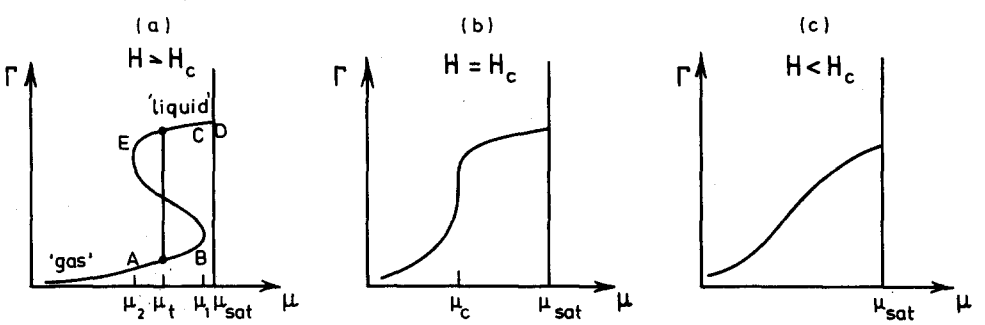

FIG. 12. Sketch of the adsorption $\Gamma(\mu)$ for three different values of H and fixed temperature in a complete wetting situation. (a) $H>H_c$. Γ exhibits a loop with spinodal points at μ_2 and μ_1. At $\mu=\mu_t$, Γ jumps discontinuously from small gas-like values to large values characteristic of the liquid. (b) $H=H_c$ the critical value. (c) $H<H_c$.

Within our present model $\Gamma(H)$ is particularly simple. Using Eq. (14), this quantity can be expressed as

$$\Gamma(H) = \pm \frac{2}{\lambda} \int_{\mu_h^w}^{\mu_h^M} d\mu_h (\rho(\mu_h) - \rho_b)(\psi(\mu_h) - \Delta p)^{-1/2} \tag{39}$$

which reduces to twice the single wall result[24] in the limit $H \to \infty$. It is straightforward to show that differentiation of Eq. (24) with respect to μ yields Eq. (39), i.e., these formulas are consistent with Eq. (38). The latter can be used to infer the behavior of $\Gamma(H)$. Numerical results for Γ as a function of $p/p_{\rm sat}$ at several values of H will be presented in Sec. IV. For a large value of H it is readily shown that $\Gamma(\mu)$ exhibits a loop; this is sketched, for a wetting situation, in Fig. 12(a). When $\Delta\mu \to 0$, $H_{\rm min} \to \infty$ (see Fig. 9). Thus no gas configuration will exist if $H < H_{\rm min}(\mu)$. As $\Delta\mu$ is increased $H_{\rm min}$ is reduced and at a certain chemical potential $\mu = \mu_1$, where $H_{\rm min}(\mu_1) = H$, a gas solution will appear. On further increasing $\Delta\mu$ both upper and lower gas branches exist for that value of H and it is this mechanism which gives the lower part of the loop in Fig. 12(a). The liquid exists for all these undersaturations. Upon increasing $\Delta\mu$ further $H_{\rm max}$ is reduced and eventually coincides with H. At this value of $\mu (= \mu_2)$ we lose the dense fluid configuration and only gas persists for $\mu < \mu_2$. This construction implies that the two singularities in $(\partial\Gamma/\partial\mu)_H$ at μ_1 and μ_2 correspond to spinodal points where $(\partial H/\partial\Delta p)_{\mu=\mu_1} = 0$ and $(\partial H/\partial\Delta p)_{\mu=\mu_2} = 0$, respectively. The argument can be formalized if we note that Eq. (37) implies that a divergence of $(\partial\Gamma/\partial\mu)_H$ is equivalent to a divergence of $\int_0^H dz(\partial\rho(z)/\partial\mu)$ and we have shown already that $(\partial\rho(z)/\partial\mu)$ is singular at a spinodal point. The first order transition will occur at some intermediate value of the chemical potential μ_t, i.e., $\mu_2 < \mu_t < \mu_1$ and Γ will jump discontinuously from a small value characteristic of a gas to a large value characteristic of adsorption from a metastable liquid. The portion of the curve with $(\partial\Gamma/\partial\mu) < 0$ in Fig. 12(a) corresponds to an unstable region.

If H is chosen to be smaller $\mu_{\rm sat} - \mu_1$ and $\mu_{\rm sat} - \mu_2$ are correspondingly larger; the loop is shifted and reduced in extent. Eventually the critical value $H = H_c$ is reached for which $\Gamma(\mu)$ no longer exhibits a loop, but rather adopts the form shown in Fig. 12(b) with $(\partial\mu/\partial\Gamma)^c = (\partial^2\mu/\partial\Gamma^2)^c = 0$. This behavior is associated with the condition expressed in Eq. (29) or Eq. (33) and and corresponds to Fig. 11(b). For $H < H_c$ Γ increases monotonically with μ [see Fig. 12(c)].

A similar analysis can be carried out for a partial wetting situation, but the case which is probably most relevant for adsorption experiments on mesoporous solids is that described in Fig. 12(a). This corresponds to "conventional" capillary condensation. If the capillary is sufficiently wide so that condensation occurs at a small value of $\Delta\mu$ we may analyze the adsorption using approximations developed earlier. The interfacial free energy of the liquid configuration is

$$\gamma_l(H) \sim (p - p_l^+)H/2 + \gamma_{sl}$$

which follows from Eq. (2) or Eq. (27). Using Eq. (38), the adsorption in this configuration is

$$\Gamma_l(H) \sim (\rho^+ - \rho_b)H + 2\Gamma_{sl}, \tag{40}$$

where ρ^+ is the density of the metastable bulk liquid and Γ_{sl} is the adsorption at a single solid–liquid interface. The interfacial free energy of the gas with wetting films is given by Eq. (28). On differentiating with respect to μ, or from direct analysis of Eq. (37), we find for small $\Delta\mu$ and large H:

$$\Gamma_{\rm wet}(H) \sim 2(\rho^+ - \rho_b)t(H) + A, \tag{41}$$

where A depends weakly on H and μ. At this level of approximation, condensation occurs when the pressure p satisfies Eq. (6). The adsorption jumps by an amount

$$\Delta\Gamma_t = [H - 2t(H)](\rho^+ - \rho_b) + 2\Gamma_{sl} - A \tag{42}$$

at the transition. Alternatively using Eq. (6), this can be reexpressed as

$$\Delta\Gamma_t \approx 2\gamma_{lg}(\rho^+ - \rho_b)/(p - p_l^+), \tag{43}$$

where we have ignored the last two terms of Eq. (42). In the same spirit as the derivation of the Kelvin equation [see Eq. (5)], we can expand the various quantities in Eq. (43) about their values at saturation to obtain

$$\Delta\Gamma_t \approx 2\gamma_{lg}/\Delta\mu \approx 2\gamma_{lg}/k_B T \ln(p_{\rm sat}/p). \tag{44}$$

This asymptotic (large H and small $\Delta\mu$) argument assumes the existence of the gas configuration. Our previous discussion showed that for a fixed finite H the latter does not extend to $\mu = \mu_{\rm sat}$; the adsorption isotherm ends in a loop at $\mu = \mu_1 < \mu_{\rm sat}$ in Fig. 12(a). We can estimate μ_1 by recalling that gas first appears when $H_{\rm min}(\mu_1) = H$, where $H_{\rm min}$ satisfies $(\partial H/\partial\Delta p)_{H=H_{\rm min}} = 0$. For small undersaturations, we can employ Eq. (21) for $H(\Delta p)$ appropriate to a wetting situation. We find $\Delta p(H_{\rm min})$ satisfies

$$0 = -\frac{1}{a_g \Delta p} + \frac{2}{a_l(\psi^+ - \Delta p)}$$

or

$$\Delta p(H_{\rm min}) = \psi^+ a_l/(2a_g + a_l).$$

Substituting this result back into Eq. (21) we obtain

$$\lambda H_{\rm min} \approx -(1/a_g + 2/a_l)\ln(\psi^+/\Theta^2), \tag{45}$$

where we have ignored terms that remain finite in the limit $\psi^+ \to 0$. Thus $H_{\rm min}$ increases logarithmically as $\mu \to \mu_{\rm sat}$ and the gas first appears for fixed H when the undersaturation is such that

$$p - p_l^+ = \frac{\Theta^2}{2\alpha} \exp[-\lambda H a_g a_l/(a_l + 2a_g)]. \tag{46}$$

This equation determines μ_1. On the other hand, the chemical potential at the first order transition for the same value of H, μ_t, corresponds to Eq. (6).

In the partial wetting situation, a similar asymptotic argument yields in place of Eq. (41), $\Gamma_g(H) \sim 2\Gamma_{sg}$, and in place of Eq. (42),

$$\Delta\Gamma_t \approx H(\rho^+ - \rho_b) + 2(\Gamma_{sl} - \Gamma_{sg}) \tag{47}$$

for the jump in adsorption at the transition. Here Γ_{sg} is the adsorption at a single solid–gas interface.

So far we have considered the adsorption isotherms $\Gamma(\mu)$ at fixed separation H. Sometimes it is useful to calculate Γ as a function of H at fixed μ and T. This quantity was calculated by Lane and Spurling[14] in a grand canonical Monte Carlo simulation of a Lennard-Jones fluid between two adsorbing walls and, more recently, by Freasier and Nordholm[16] in a

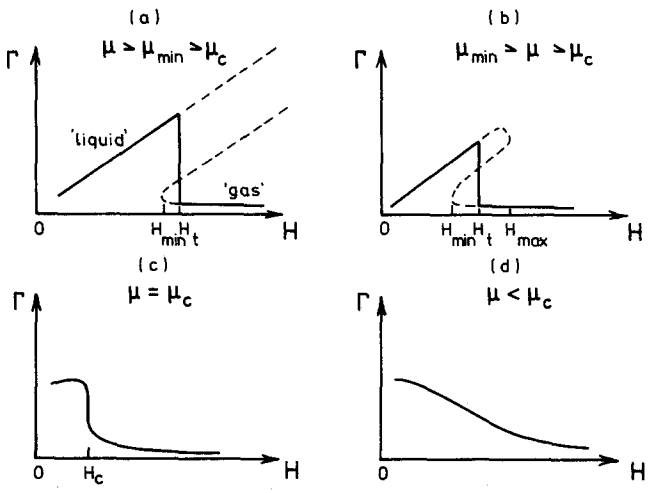

FIG. 13. Sketch of the adsorption $\Gamma(H)$ for four different chemical potentials μ and fixed temperature in a complete wetting situation. (a) $\mu_{sat} > \mu > \mu_{min} > \mu_c$. Γ jumps discontinuously at $H = H_t$ from small gas values to values appropriate to a liquid. On the liquid branch $\Gamma \sim (\rho^+ - \rho_b)H$ for large H. The dashed lines mark metastable or unstable solutions. (b) $\mu_{min} > \mu > \mu_c$. The jump in Γ at $H = H_t$ is smaller now and the metastable solution ends at $H = H_{max}$. (c) $\mu = \mu_c$ the critical value. (d) $\mu < \mu_c$.

density functional treatment of the same system. The form of $\Gamma(H)$ depends on μ and T and can be ascertained from Figs. 7–10. In Fig. 13 we sketch $\Gamma(H)$ for four different values of μ and a fixed temperature, corresponding to a complete wetting situation. For small $\Delta\mu$ and large H, the adsorption on the lower gas branch is given by Eq. (41) and that on the liquid branch by Eq. (40). The gas branch is stable at large H and we expect $\Gamma_{wet}(H)$ to increase slowly as H is reduced; the film thickness $t(H)$ increases slowly with decreasing H [see Eq. (22)]. At $H = H_{min}$, $\Delta p(H)$ exhibits a turning point [Fig. 9(b)] and this leads to an equivalent turning point in $\Gamma(H)$ where $(\partial\Gamma(H)/\partial H)_{H=H_{min}}$ is singular. This can be understood by writing

$$\left(\frac{\partial\Gamma}{\partial H}\right)_{\mu,T} = \left(\frac{\partial\Gamma}{\partial\Delta p}\right)_{\mu,T}\left(\frac{\partial\Delta p}{\partial H}\right)_{\mu,T} = \left(\frac{\partial\Gamma}{\partial\mu_h^M}\right)_{\mu,T}\left(\frac{\partial\Delta p}{\partial H}\right)_{\mu,T}\Bigg/\left(\frac{\partial\Delta p}{\partial\mu_h^M}\right)_{\mu,T}$$

and noting that $(\partial\Gamma/\partial\mu_h^M)$ and $(\partial\Delta p/\partial\mu_h^M)$ are finite and nonzero at $H = H_{min}$. Beyond the turning point $\Gamma(H)$ increases with increasing H as shown by the dotted line in Fig. 13(a). The variation is linear at large H since this corresponds to the unstable gas branch. On the liquid branch $\Gamma(H)$ also increases linearly with H for large H with a slope equal to $(\rho^+ - \rho_b)$. This branch is metastable until $H = H_t$ [see Fig. 10(c)] but becomes the stable branch for $H < H_t$. Thus $\Gamma(H)$ jumps discontinuously by the amount $\Delta\Gamma_t$ given by Eq. (42), or Eq. (43) or Eq. (44), if the conditions for the validity of the latter are met at $H = H_t$. Such a jump, from low values of Γ characteristic of adsorption from a gas, to large values, increasing linearly with H, characteristic of adsorption from a *metastable* liquid, is a clear signature of capillary condensation. Lane and Spurling found this behavior[35] in their simulations (see Fig. 3 of Ref. 14). Freasier and Nordholm calculated $\Gamma(H)$ similar[36] to that shown in Fig. 13(a), but without the unstable portion. Neither group appears to have made the connection with the "classical" treatment of capillary condensation that we present here.

For a larger value of $\Delta\mu$: $\mu_{min} > \mu > \mu_c$ the dense fluid branch of $\Gamma(H)$ ends at $H = H_{max}$, where $(\partial\Gamma/\partial H)$ is singular [see Fig. 13(b)]. H_t is smaller than previously and the magnitude of the jump is reduced, but $\Gamma_l(H)$ should retain a roughly linear dependence on H. Wetting films will no longer arise for these undersaturations. When $\mu = \mu_c$, the critical value for the given T, the loop in $\Gamma(H)$ disappears and $(\partial\Gamma/\partial H)$ diverges at $H = H_c$ [see Fig. 13(c)]. If $\mu < \mu_c$, we expect adsorption of the type shown in Fig. 13(d).

The case of partial wetting has some features in common with that of complete wetting. For small $\Delta\mu$ the jump in adsorption is now given by Eq. (47) with H_t determined, approximately, by Eq. (4) or Eq. (5). Γ_l still increases linearly with H.

A quantity which is closely related to the adsorption is $f(H)$, the force per unit area of wall arising from solid–fluid and fluid–fluid interactions. We apply this force externally to the walls and adopt the convention that f is positive when the walls repel each other.[14] $f(H)$ is sometimes called the solvation force. It is obtained thermodynamically from the relation

$$(\partial\Omega/\partial V)_{\mu,T,A_{sf}} \equiv -p - f(H). \tag{48}$$

In a bulk system the derivative must reduce to $-p$, the negative of the pressure so the surface contribution $f(H)$ must vanish as $H \to \infty$. Using Eq. (1) it follows that

$$f(H) = -2[\partial\gamma(H)/\partial H]_{\mu,T} \tag{49}$$

which is consistent with Ref. 15. A surface Maxwell relation[15,37] can now be obtained by use of Eq. (38), i.e.,

$$\left(\frac{\partial\Gamma}{\partial H}\right)_{T,\mu} = -2\left(\frac{\partial^2\gamma}{\partial H\partial\mu}\right)_T = \left(\frac{\partial f}{\partial\mu}\right)_{T,H}. \tag{50}$$

In our present theory, $f(H)$ reduces to

$$f(H) = -\frac{1}{2\alpha}(\Delta p(H) - 4\epsilon_w^2 e^{-\lambda H}), \tag{51}$$

where we have used Eq. (25). Thus a knowledge of $\Delta p(H)$ is sufficient to determine the force. Of course our theory will not produce the oscillatory forces[14] characteristic of dense liquids held between two plates at small separation. Oscillations in $f(H)$ arise from the short-ranged correlations[16] which are absent from our theory. Nevertheless, our approach should be sufficiently realistic to provide useful information about the variation of f expected at a phase transition or for large H.

For example on the stable gas branch $\Delta p(H)$ decays exponentially as $H \to \infty$ [see Eq. (26)], so the force is small and negative (weakly attractive) at large H. By contrast on the liquid branch $\Delta p(H) \to \psi^+$ as $H \to \infty$ so $f(H) \to -(p - p_l^+)$, a negative constant. If capillary condensation occurs at a large value of H then the force should be reduced discontinuously by an amount $\Delta f_t \simeq p_l^+ - p$, which is given in turn by Eq. (4) or Eq. (6). This situation is described in Fig. 14; it corresponds to the adsorption shown in Fig. 13(a). In their calculations, Lane and Spurling[15] and

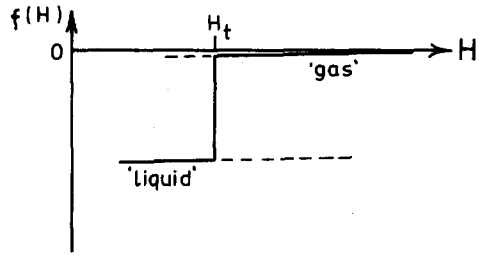

FIG. 14. Sketch of the force per unit area $f(H)$ corresponding to Fig. 13(a). f falls discontinuously by an amount $\sim(p_l^+ - p)$ at $H = H_t$. The dashed lines indicate metastable solutions.

Freasier and Nordholm[16] find a discontinuity in $f(H)$ at $H = H_t$, and $\Delta f_t \equiv f_l(H_t) - f_g(H_t)$ is negative, as is predicted here. We believe that this argument lends further support to our suggestion that these authors were indeed observing the same phenomenon, i.e., capillary condensation.

$f(H)$ can be calculated for all the other examples. At a capillary critical point, $-f(H)$ would be similar to $\Delta p(H)$ plotted in Fig. 11(b); $(\partial H/\partial f) = (\partial^2 H/\partial f^2) = 0$ for $\mu = \mu_c$ and $H = H_c$. In reality singularities in $(\partial f/\partial H)_\mu$ may be masked by the presence of oscillations at small H.

IV. RESULTS OF CALCULATIONS

In this section we present some numerical results for a model capillary characterized by a wall potential with $\epsilon_w = 2.114 k_B T_c$. This is the model system considered earlier.[26] Our calculations were based on the Carnahan and Starling equation of state for hard spheres

$$p_h(\rho) = k_B T \rho (1 + \eta + \eta^2 - \eta^3)/(1 - \eta)^3 \tag{52a}$$

and

$$\mu_h(\rho)/k_B T = \ln \eta + \eta(8 - 9\eta + 3\eta^2)/(1 - \eta)^3, \tag{52b}$$

where $\eta = \pi\rho d^3/6$ is the packing fraction and d is the hard sphere diameter. The critical density ρ_c and temperature T_c of the bulk fluid then satisfy[24]

$$\rho_c d^3 = 0.249, \quad \alpha = 11.102 k_B T_c d^3. \tag{53}$$

The transition from partial wetting to complete wetting ($\theta = 0$) occurs (for a single wall) when the minimum of the function $I(\mu_h)$ coincides with the second minimum of ψ, i.e., μ_h^+, at bulk coexistence (see Fig. 7 and 9). Thus, $2\epsilon_w = \alpha\rho_l(T_W)$ determines the wetting temperature.[24] For the above choice of ϵ_w, $T_W = 0.96 T_c$. The wetting transition is a second order phase transition in Sullivan's model[25] so there is no thick–thin film (prewetting) transition.[23] Increasing ϵ_w at fixed α reduces T_W/T_c. We chose a small value of ϵ_w, and hence a high value of T_W/T_c, in order that we could investigate easily the phase equilibria over a large temperature range in particular temperatures near T_s where the contact angle $\theta = \pi/2$, i.e., $\gamma_{sg}(T_s) = \gamma_{sl}(T_s)$. In these circumstances, liquid and gas coexist at $\mu = \mu_{sat}$ and $H = \infty$.[26] $T_s = 0.57 T_c$ for the above choice of ϵ_w. (The triple point temperature for an argon-like fluid is roughly $0.5 T_c$.)

All the features described in Figs. 2, 4, and 7–11 were confirmed by the numerical results. Capillary coexistence curves such as that sketched in Fig. 6 were also computed.

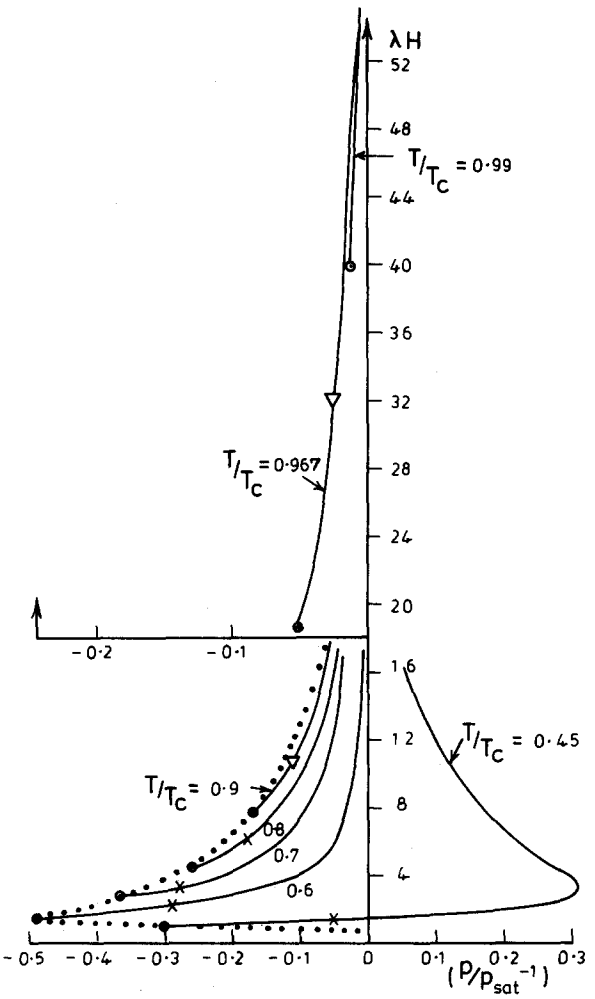

FIG. 15. Capillary coexistence curves, at different reduced temperatures T/T_c, as a function of the gas pressure p. The results for $T = 0.99 T_c$ and $0.967 T_c$ are plotted on an expanded pressure scale. For the supersaturated fluid at $T = 0.45 T_c$ p is p_g^+. ∇ denote the end of bulk two phase region. $\times$ denote the cross-over points. The dotted line marks the line of critical points $\odot$.

The phase equilibria for this model is summarized in Fig. 15 where we plot lines of coexistence of two fluid phases in the (H,p) plane for several different temperatures, above and below T_W. These lines terminate in capillary critical points at $H = H_c(T)$ and $p = p_c(T)$. If $p < p_c(T)$ or $H < H_c(T)$, only one fluid phase can exist in the capillary. For very small undersaturation, the lines follow the prediction of the Kelvin equation (5) or Laplace equation (4), so that $(p - p_{sat}) \propto -1/H$, provided $T > T_s$. If $T < T_s$, then $\cos\theta < 0$ and the Laplace equation is replaced by

$$p - p_g^+ = -2\gamma_{lg}\cos\theta/H, \tag{54}$$

where p_g^+ is the pressure of the metastable gas, with density ρ_g^+, at the same chemical potential μ as the bulk liquid ($\mu > \mu_{sat}$). The right-hand side of Eq. (54) is then the pressure difference across a *convex* meniscus in the slit. The analog of the Kelvin equation is

$$k_B T \ln(p_g^+/p_{sat}) = -2\gamma_{lg}\cos\theta/H(\rho_l - \rho_g), \tag{55}$$

where we have approximated $\mu - \mu_{sat}$ by

where we have approximated $\mu - \mu_{sat}$ by $k_B T \ln(\rho_g^+/\rho_g) \approx k_B T \ln(p_g^+/p_{sat})$ and the coexistence curve for $T = 0.45T_c$ in Fig. 15 follows this prediction[26] for very small $p_g^+ - p_{sat}$.

For $T \lesssim 0.7T_c$, the Kelvin equation is accurate to a few percent for $\lambda H \gtrsim 14$ corresponding to undersaturations of 5% or less (see also Ref. 26). For higher temperatures the Laplace form is more appropriate since the gas is no longer close to ideal and, for $T < T_W$, this is fairly accurate for $\lambda H \gtrsim 25$, or undersaturations of 3% or less. In the complete wetting regime $T > T_W$, the deviations of the numerical results from those predicted by the unmodified Kelvin or Laplace equations are rather large even for $\lambda H \sim 100$ or undersaturations of about 0.3%. Including the effects of wetting layers via Eq. (6) reduces the discrepancies, but it is clear that macroscopic or semimacroscopic equations are quantitatively accurate only at very small undersaturations in a complete wetting situation.[38] In this context it is important to recall that the macroscopic description is only appropriate when $\mu < \mu_{min}$ in Fig. 3(a) so that a mestatable bulk liquid exists. At high temperatures, the van der Waals loop in $\mu(\rho)$ shrinks and $(\mu_{sat} - \mu_{min}) \to 0$. This automatically restricts the use of the Laplace and Kelvin equations, or their modifications, to small undersaturations. The pressure corresponding to μ_{min} is indicated by a triangle for $T = 0.967T_c$ and $0.9T_c$ in Fig. 15.

At lower temperatures $T < T_W$, the cross-over mechanism described in Sec. III comes into play and we have indicated the cross-over values[30] H_{co} by crosses. As mentioned earlier, in Ref. 26 we identified the cross-over points with the capillary critical points for $T \lesssim 0.6T_c$. In reality the coexistence lines extend to smaller H and p, as is shown in Fig. 15.

The line of critical points, marked by dots, has an interesting shape which can be explained by means of a simple slab approximation for the density profiles of the fluid in the capillary. We digress a little to elucidate this.

In the neighborhood of the capillary critical point we find from our numerical results that the profiles $\rho(z)$ have similar shapes but different midpoint densities ρ^M. Often the profiles are rather flat. These considerations lead us to a crude slab approximation in which we take the profile to be constant: $\rho(z) = \rho^M$ for $0 < z < H$. Clearly such a model is inappropriate for describing coexistence of liquid and gas at large H—especially in the case of complete wetting but becomes more realistic for small separations. The grand potential, per unit area of a single wall, follows[6] from Eq. (7):

$$\omega(\rho^M) = H(f_h(\rho^M) - \alpha\rho^{M2}/2 - \mu\rho^M) + \rho^M(\alpha\rho^M - 4\epsilon_w)(1 - e^{-\lambda H})/2\lambda. \quad (56)$$

The equilibrium solution is that which minimizes ω at fixed μ, T, and H. Thus we require

$$\left(\frac{\partial\omega}{\partial\rho^M}\right)_{\mu,T,H} = 0 = H(\mu_h(\rho^M) - \alpha\rho^M - \mu) + (\alpha\rho^M - 2\epsilon_w)(1 - e^{-\lambda H})/\lambda. \quad (57)$$

For a bulk fluid only the first term is relevant and the bulk density ρ_b is determined, as usual, from the roots of $\mu = \mu_h(\rho_b) - \alpha\rho_b$. In the capillary, the second term becomes important. It is convenient to rewrite Eq. (57) as

$$\mu_h(\rho^M) - \alpha\rho^M(1 - (1 - e^{-\lambda H})/\lambda H) = \mu + 2\epsilon_w(1 - e^{-\lambda H})/\lambda H \quad (58)$$

and plot the various terms as a function of ρ^M (see Fig. 16). The fluid–fluid contribution $\alpha\rho^M(1 - e^{-\lambda H})/\lambda H$ reduces the net attraction so that the effective value of α is smaller in the capillary. This terms acts to smear out the minimum in the van der Waals loop [Fig. 16(a)] and for smaller values of H will remove the minimum, driving the fluid towards criticality [Fig. 16(b)]. The solid-fluid contribution $2\epsilon_w(1 - e^{\lambda H})/\lambda H$ shifts the effective chemical potential. Thus it is possible to choose $\mu < \mu_{min}$, so that the bulk fluid is outside the two-phase region, and still find multiple roots of Eq. (58), as illustrated in Fig. 16(a). If the solutions have equal grand potential they correspond to coexisting fluid configurations with distinct values of ρ^M. For a certain value of $H (= H_c)$ the multiple roots merge into a single critical value ρ_c^M as shown in Fig. 16(b). The corresponding critical value of $\mu (= \mu_c)$ is determined by Eq. (58); this may also satisfy $\mu_c < \mu_{min}$.

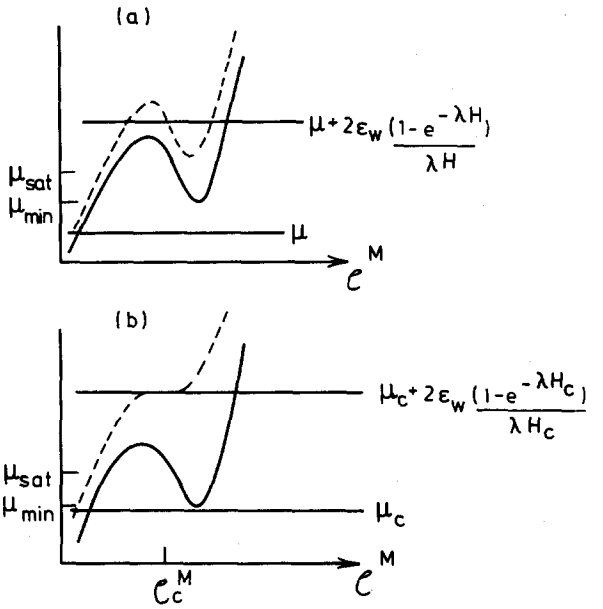

FIG. 16. Sketch of various terms in Eq. (58). Solid curve: $\mu(\rho^M) = \mu_h(\rho^M) - \alpha\rho^M$. Dashed curve: $\mu(\rho^M) + \alpha\rho^M(1 - e^{-\lambda H})/\lambda H$. The intersections of the dashed curve in (a) with the horizontal line $\mu + 2\epsilon_w(1 - e^{-\lambda H})/\lambda H$ give possible equilibrium values of the density ρ^M. In (b) the intersection at the point of inflection yields the critical density ρ_c^M and chemical potential μ_c. These plots refer to a high temperature. At low temperatures the loop in $\mu(\rho^M)$ is more pronounced and $\mu_c > \mu_{min}$.

The critical density and separation are determined, for a given temperature, by the conditions

$$\frac{\partial}{\partial\rho^M}(\mu_h(\rho^M) - \alpha_{eff}(H)\rho^M) = \frac{\partial^2}{\partial\rho^{M2}}(\mu_h(\rho^M) - \alpha_{eff}(H)\rho^M) = 0.$$

Since $\alpha_{eff}(H) \equiv \alpha(1 - (1 - e^{-\lambda H})/\lambda H)$ does not depend on ρ^M, the second of these conditions reduces to $(\partial^2\mu_h/\partial\rho^{M2}) = 0$, which is identical to that which deter-

mines the *bulk* critical density ρ_c. It follows that $\rho_c^M = \rho_c = 0.249d^{-3}$ is independent of T and H in this slab approximation. The critical separation follows from the first condition:

$$k_B T\left(\frac{\partial M}{\partial \rho}\right)_{\rho=\rho_c^M} - \alpha_{\rm eff}(H_c) = 0, \tag{59}$$

where $M(\rho) \equiv \mu_h(\rho)/k_B T$ is a function of ρ only. But the bulk critical density satisfies

$$k_B T_c\left(\frac{\partial M}{\partial \rho}\right)_{\rho=\rho_c} - \alpha = 0, \tag{60}$$

so we combine these results to obtain

$$\frac{T}{T_c} = \alpha_{\rm eff}(H_c)/\alpha = 1 - (1 - e^{-\lambda H_c})/\lambda H_c \tag{61}$$

which determines H_c for a given T. Alternatively, this equation determines the capillary critical temperature $T_c^{\rm cap}$ for a given separation H.

In the limit $\lambda H \gg 1$, Eq. (61) implies

$$\frac{T_c - T_c^{\rm cap}}{T_c} \sim 1/\lambda H, \tag{62}$$

i.e., the critical temperature is reduced below its bulk value by a term inversely proportional to the wall separation. However, as mentioned above, our slab approximation is not reliable for very large H. As $H \to \infty$ and $T_c^{\rm cap} \to T_c$, the effects of bulk criticality will manifest themselves and the details of the shape of the profile become important. Consequently, Eq. (62) may not give the correct asymptotic behavior.[39] This could be obtained from a detailed analysis of the full differential equation for the density profile. From their mean-field treatment of critical temperature shifts, Nakanishi and Fisher[17] predict

$$\frac{T_c - T_c^{\rm cap}}{T_c} \sim \frac{1}{H^2} \quad (H \to \infty) \tag{63}$$

but this might not be the only possibility.[51] It is interesting to note that shifts of the type indicated by Eq. (62) were found for films of *intermediate* thickness by Nakanishi and Fisher (see Fig. 10 of Ref. 17).

The chemical potential at the capillary critical point is

$$\mu_c = \mu_h(\rho_c^M) - \alpha\rho_c^M + (\alpha\ \rho_c^M - 2\epsilon_w)(1 - e^{-\lambda H_c})/\lambda H_c,$$

which, using Eq. (61), reduces to

$$\mu_c = \mu_h(\rho_c^M) - \alpha\rho_c^M\, T/T_c - 2\epsilon_w(1 - T/T_c)$$

or, in terms of the bulk critical chemical potential $\mu_c^b(T_c)$:

$$\mu_c = (\mu_c^b(T_c) + 2\epsilon_w)T/T_c - 2\epsilon_w. \tag{64}$$

Again this result may not give the correct limiting behavior at $T \to T_c$. We have used Eq. (64) along with Eq. (61) to construct the line of critical points shown in Fig. 17. Although the slab approximation tends to underestimate the length of the coexistence lines, it is clear from a comparison with the dotted curve in Fig. 15 that the overall shape of the line of critical points is well represented. Moreover, the prediction that $\rho_c^M d^3 = 0.249$ is reasonably well obeyed; the critical midpoint densities obtained from the full calculations are roughly constant and take values close to the above for a wide range of temperatures and different choices of ϵ_w.

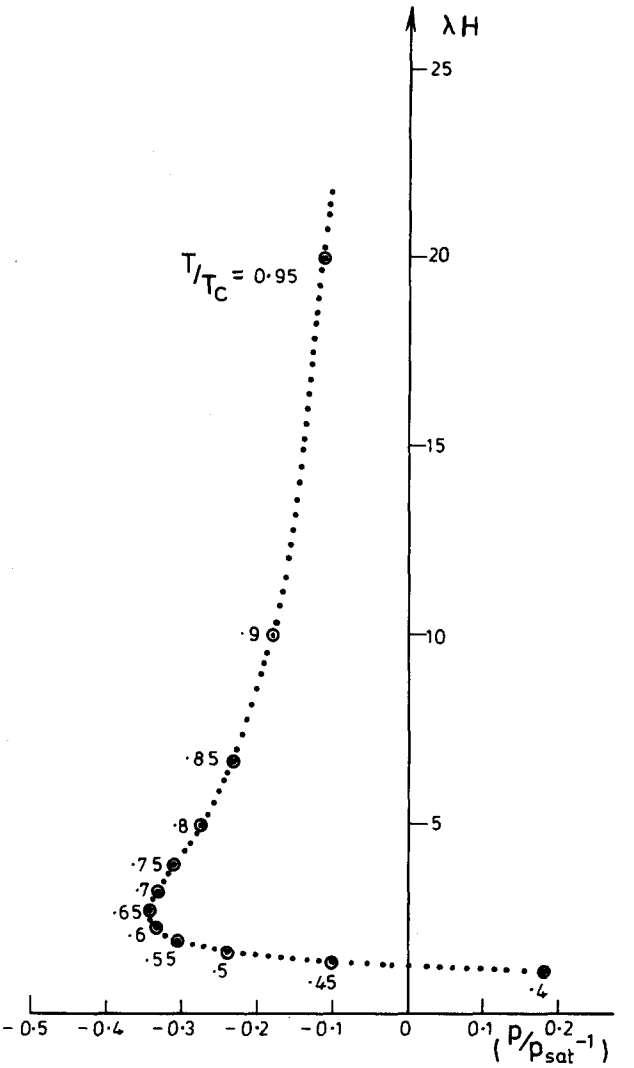

FIG. 17. The line of capillary critical points ⊙ calculated from the slab approximation for various temperatures T/T_c. The dotted curve is a guide to the eye. For the supersaturated fluid p is p_g^+,

At low temperatures and small λH there is a turning point in the line of critical points; this occurs for $T/T_c \sim 0.65$. At lower temperatures $p_{\rm sat}(T) - p_c(T)$ decreases and eventually becomes positive. Such behavior can be understood from Fig. 16. The van der Waals loop becomes more pronounced as T is lowered so criticality cannot be achieved if $\mu < \mu_{\rm sat}$. (λH is already very small.) Thus $\mu_c \to \mu_{\rm sat}$ and, eventually at very low temperatures, $\mu_c > \mu_{\rm sat}$. Note also that for $T \to T_s = 0.57T_c$, $\cos\theta \to 0$ so that Eq. (4) predicts that coexistence can only occur for very small undersaturations.

We return finally to the isotherm $T = 0.45T_c < T_s$ in Fig. 15. This exhibits a loop for small values of H; other isotherms for T/T_s show similar structure.[26] As mentioned above, the coexistence line follows the prediction of the appropriate Kelvin equation (55) at large H, but for smaller separations the H dependence of $\gamma(H)$ becomes very significant and produces the loop. The interfacial free energy of the liquid, γ_l decreases as $-e^{-\lambda a_l H}$, whereas that of the gas γ_g decreases as $-e^{-\lambda a_g H}$. From its definition, it is straightfor-

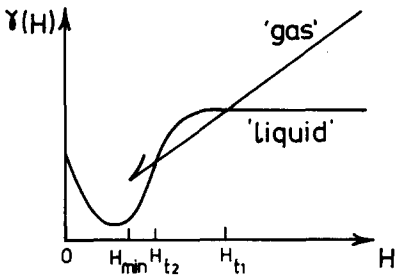

FIG. 18. Sketch of $\gamma(H)$ for a supersaturated fluid at temperature $T<T_s$. The pressure is chosen so that two first order transitions occur at separations H_{t1} and H_{t2}.

ward to show that $a_l=(1+\alpha\kappa_T\rho_l^2)^{-1/2}$, where κ_T is the isothermal compressibility of the bulk liquid. The corresponding relation holds for the gas. Since $\rho_l \gg \rho_g$ at low temperatures it follows that $a_l \ll a_g$ and γ_l decreases much more rapidly than γ_g. A sketch of $\gamma(H)$ is shown in Fig. 18. The gas is now supersaturated so $\gamma(H)$ increases linearly with H at large H on this branch. Liquid is stable for $H>H_{t1}$ and a first order transition to gas occurs at $H=H_{t1}$. The gas remains the stable configuration for $H_{t2}<H<H_{t1}$, but then a further first order transition to liquid occurs at $H=H_{t2}$. Such behavior will occur if $T<T_s$, provided $p(T)>p_{\rm sat}(T)$ and $p_{\rm max}(T)>p(T)>p_c(T)$, where $p_{\rm max}(T)$ is the pressure at which $dH/dp=\infty$ and $p_c(T)$ is the pressure at the capillary critical point. If $p(T)>p_{\rm max}(T)$, the liquid remains stable for all H. If $p_c(T)>p(T)>p_{\rm sat}(T)$, there is a single transition from liquid to gas as H is reduced. The asymmetry of the isotherms in Fig. 15, as a function of $p-p_{\rm sat}$, is a consequence of the difference in densities between liquid and gas and of the exponential-type forces assumed in our model.

The adsorption was calculated as a function of μ for different values of H and several temperatures. Specimen results are plotted in Figs. 19 and 20. In order to display the condensation and its dependence on H, we found it convenient to plot a modified adsorption

$$\Gamma_M=\frac{d^3}{H}\int_0^H dz\rho(z)$$

rather than the excess function $\Gamma(H)$ defined in Eq. (37). Γ_M is dimensionless. We also found it convenient to measure the degree of undersaturation by the ratio of densities ρ_b/ρ_g; ρ_b is the density of the bulk gas at the given chemical potential and ρ_g is the density of the gas at saturation. Figure 19 shows the results for T slightly greater than T_W; this corresponds to the situation described schematically in Fig. 12. For the smallest separation $\lambda H=14$, Γ_M increases monotonically

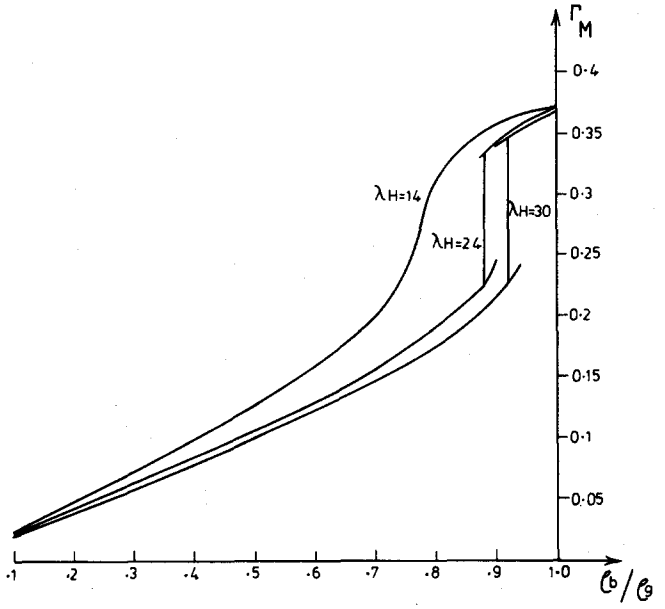

FIG. 19. Adsorption Γ_M vs undersaturation, expressed as a ratio of densities, for three different separations H and a fixed temperature $T=0.97T_c$, above T_W. The vertical lines represent the jump in adsorption at the first order transition. Note the small metastable portions of Γ_M.

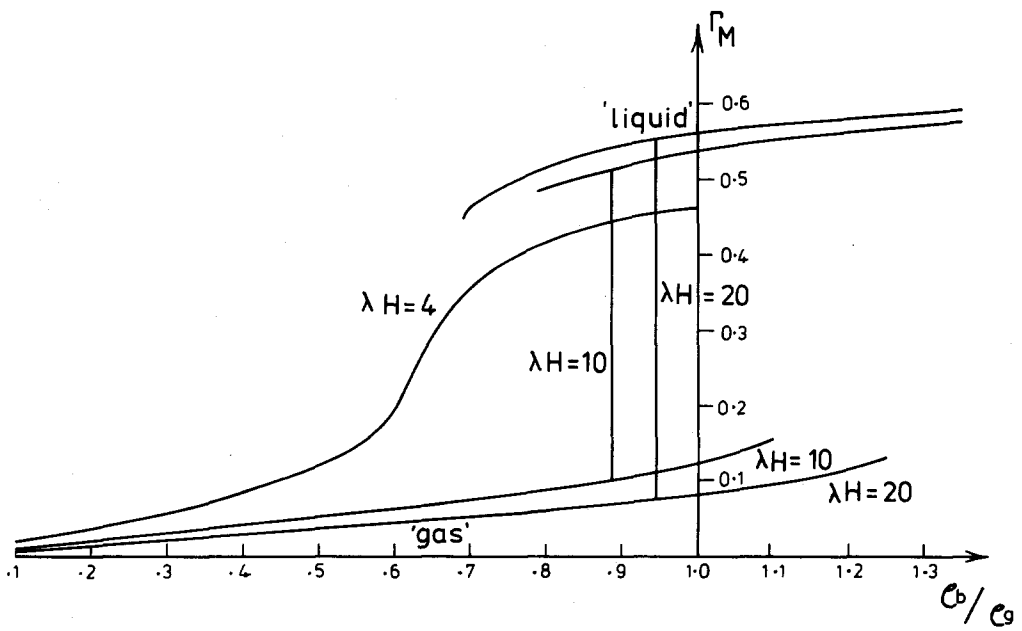

FIG. 20. The same as in Fig. 19 but for $T=0.8T_c$, which is below T_W. The metastable portion of Γ_M on the gas branch extends to supersaturation now. For the supersaturated fluid ρ_b is ρ_g^+.

with ρ_b/ρ_g as is appropriate to a supercritical isotherm. The other values of λH correspond to subcritical isotherms and exhibit loops. The metastable portions of the latter are shown. Γ_M and, hence Γ, jump by a finite amount at the first order transition. The larger the value of H the closer is the transition to saturation and the larger is the jump $\Delta\Gamma_t$, as is indicated by Eqs. (42)–(44). In Fig. 20 results for $T < T_W$ are plotted. These are similar to those for $T > T_W$ except that the gas branch now extends to $\mu = \mu_{sat}$ and beyond. The isotherm should be contrasted with that sketched in Fig. 12(a) which has a spinodal point at $\mu = \mu_1 < \mu_{sat}$ and with those shown in Fig. 19. Examination of Fig. 7 shows that a gas solution persists to $\mu = \mu_{sat}$. Only upon supersaturating the bulk fluid is it possible to reach the spinodal point of the gas branch, beyond which it is no longer possible to find gas configurations for the given H and T. This is indicated for $\lambda H = 10$ and 20 in Fig. 20. The liquid is stable for all $\mu > \mu_{sat}$ for this temperature.

V. DISCUSSION

Our model, which is probably the simplest realistic model for an inhomogeneous three-dimensional fluid that one might contemplate, provides considerable insight into the phase equilibria of a fluid confined in a narrow capillary. We expect that many of our results will have validity beyond this particular model whilst others are certainly specific to it. The overall shape of the lines of coexistence (Fig. 15) is probably generic—with the possible exception of the low temperature region. Whether or not loops in the coexistence lines should occur for supersaturated fluids depends on the details of $\gamma(H)$ at small H. These depend, in turn, on the choice of solid–fluid and fluid–fluid potential functions. It is feasible that for certain choices loops would arise for an undersaturated fluid but this remains to be investigated. Our identification of two separate mechanisms for first order transitions should also be rather general. At small undersaturations the transition is from gas to the metastable bulk liquid with the relevant branches of $\gamma(H)$ being unconnected. Such a transition is well-described by the classical, macroscopic arguments for capillary coexistence. The second mechanism does not follow from any macroscopic treatment but occurs at larger undersaturations and requires a loop in $\gamma(H)$ and in other quantities. The subsequent description of the first-order transition is then closely akin to the classical van der Waals treatment of bulk liquid–gas coexistence—provided the correct variables are chosen. The two mechanisms merge smoothly into each other, however, by closure of the loop in $\gamma(H)$ at $H = \infty$ at the bulk spinodal for $T > T_W$ and by the cross-over mechanism for $T < T_W$. Consequently, the lines of coexistence in Fig. 15 continue smoothly through these points to terminate at capillary critical points. The latter are always associated with the vanishing of loops, irrespective of whether $T >$ or $< T_W$. As expected[17] for a system of finite thickness the wetting transition that occurs for a semi-infinite system at bulk coexistence, has no *direct* relevance for the line of critical points which varies smoothly with temperature. Indeed for $T > T_W$, the critical point always occurs for a chemical potential $\mu_c < \mu_{min}$ (see Fig. 16 and the discussion of Figs. 9 and 10), i.e., outside the bulk

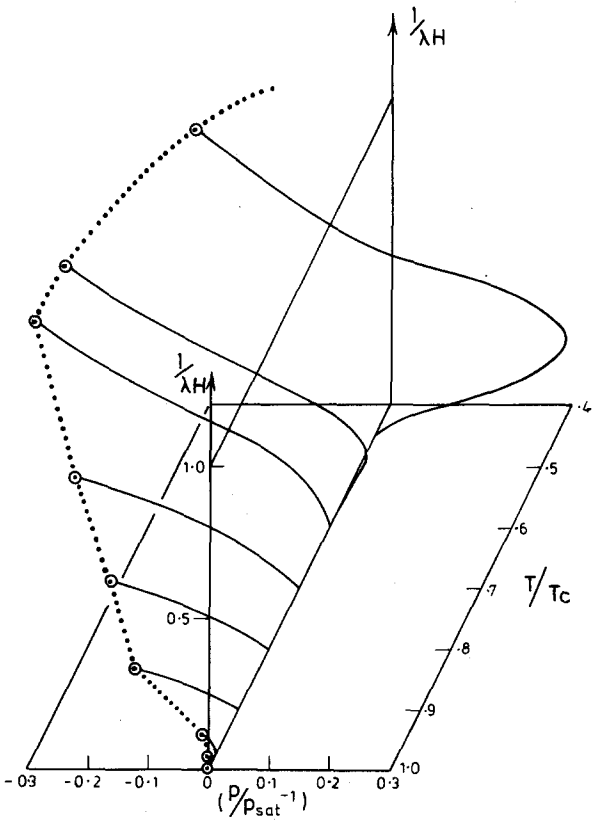

FIG. 21. Capillary phase diagram in terms of temperature T, pressure p, and the inverse of the wall separation H. The solid curves are coexistence curves at fixed T. The dotted curve marks the line of critical points ⊙. For the supersaturated fluid at the lowest temperatures p is p_g^+.

two-phase region (spinodal).[40] Thus no thick wetting films can be present at a capillary critical point; there is no metastable bulk liquid at $\mu = \mu_c$. Stable wetting films *will* occur in capillaries but, as shown in Sec. III C, only for very large H and very small undersaturation. These conditions can be realized in experiments on capillary rise,[5,6,12,41] but are unlikely to be realized in most adsorption experiments on mesoporous solids. Condensation to the liquid will usually occur at undersaturations greater than those required for the formation of thick wetting films.

The surface of first-order transitions is drawn in the phase diagram (Fig. 21); it is bounded by the line of critical points. By choosing as ordinate $1/\lambda H$, rather than λH, we emphasize the low T, small H portion of the diagram. The coexistence lines shrink to zero as $T \to T_c$. Can Fig. 21 be regarded as generic? While we have not made an exhaustive study, covering all possible choices of the parameter ϵ_w, we believe Fig. 21 is properly representative[42] of a system that undergoes a second-order (critical) wetting transition. In less restricted model systems and at real solid–fluid interfaces[23] the wetting transition is more likely to be first-order, as proposed originally by Cahn[43] and by Ebner and Saam.[44] Accompanying such a transition is a thick–thin film or prewetting transition which occurs for weakly undersaturated fluids and $T > T_W$. The prewetting transition will certainly occur in a capillary[17] when H is sufficiently large. At smaller H it will be in competition with capillary condensation. We are currently investigating models for which the fluid–fluid

and solid–fluid potentials have different range and which yield prewetting transitions, in order to determine the influence of prewetting on the form of the capillary phase diagram.[45] Long-ranged (algebraically decaying) forces are known to play a crucial role in wetting transitions and related phenomena.[23,46] It is unlikely that they will drastically alter the general features of the capillary phase diagram, but they might introduce important quantitative changes in the coexistence line, as discussed in Sec. II and Refs. 5, 6, and 12, for $T > T_w$ and large H.

We are not the first to find capillary critical points. Nicholson[11] determined a critical radius in his lattice-gas calculations of adsorption in cylindrical pores. He did not emphasize the importance of loops and metastable states, however. The latter were discussed earlier by Hill,[10] but he did not mention criticality. Our work clarifies the nature of the critical points and makes connection with the studies of Nakanishi and Fisher.[17] Although these authors employ different models and different methods of analysis their critical points are also associated with shrinking loops and merging capillary spinodals. One important difference between our mean-field density functional and Nakanishi and Fisher's Landau free energy functional is that the latter has lattice-gas symmetry. Our results, especially at low temperature, depend strongly on the asymmetry between liquid and gas arising from the large difference in density between the two bulk phases. It is this which determines the interesting shape of the coexistence lines near $T = T_s$. By contrast, lattice gas symmetry implies $\gamma_{sl} = \gamma_{sg}$, or $\cos\theta = 0$, for *all* temperatures when the surface field or contact interaction $h_1 = 0$.

Our simple free-energy functional, like continuum Landau theory, omits short-ranged correlations; the density profiles do not mimic the local ordering that occurs in more realistic treatments[9(b)] of fluids near walls. For wall separations $H \gg d$, the hard sphere diameter, we do not expect the phase equilibria to be strongly dependent on the approximation used to treat short-ranged correlations and the present local density treatment should be adequate. When $H > d$, however, packing considerations become dominant, the local approximation is very poor and more sophisticated treatments are required.[47] At low temperatures, but still above the bulk triple point, crystalline ordering may occur. In addition two-dimensional-like phase equilibria should develop when the wall separation becomes sufficiently small. Our present model functional is not designed to tackle such problems; a discrete lattice gas model is probably better suited. How realistic then are our results for small λH? We are of course at liberty to choose λ arbitrarily small which corresponds to infinite ranged potential functions. In practice it is difficult to contemplate a range λ^{-1} much greater than two or three hard sphere diameters if one is attempting to model a real fluid. Thus the details of the phase equilibria for $\lambda H \lesssim 2$ could certainly be altered in a more realistic theoretical treatment.

Do our results have any consequence for adsorption experiments on real porous solids or for computer simulations of adsorption between two walls? From our calculations it is evident that the macroscopic Kelvin equation, and simple extensions of this, give an inaccurate estimate of the pressure at which capillary condensation occurs except for very small undersaturations and, hence, large H. The deviations are especially large for $T > T_w$, the complete wetting situation. Near a capillary critical point the macroscopic description of the first order transition as condensation to a metastable bulk liquid is invalid. Further work is required, with more realistic potential functions and model capillaries, e.g., cylinders, to determine the systematics of the corrections to the classical formulas, but our present estimates (see Sec. IV) should provide useful guidelines.

Several of our theoretical predictions could be tested by simulation. We have already mentioned the work of Lane and Spurling[14,15] who found the first order transition. The adsorption $\Gamma(H)$ and the force $f(H)$ must vary in the characteristic fashion described in Sec. III E and Figs. 13 and 14 at such a transition. A critical point might be more difficult to locate [Fig. 13(c)]. An interesting case arises for the supersaturated bulk fluid at low temperatures $T < T_s$. Now one is adsorbing from a dense liquid at large H. Figure 15 suggests that for an appropriate fixed $p > p_{sat}$, *two* first-order transitions can occur as H is reduced, i.e., from liquid to gas to liquid. $\Gamma(H)$ and $f(H)$ would jump discontinuously twice. van Megen and Snook[13] have obtained adsorption isotherms similar to those plotted in Figs. 19 and 20, but without metastable portions, in Monte Carlo calculations. It would be of some interest to examine the accuracy of approximations for the jump in adsorption $\Delta\Gamma_t$ such as those given by Eqs. (42)–(44) and the corresponding formulas for the change in $f(H)$.

$f(H)$ is an important quantity because it can be measured for fluids between mica "plates" using the technique developed by Tabor, Israelachvili and others.[48] It should be possible to study first order transitions in weakly undersaturated gases by monitoring jumps in $f(H)$. In principle it should also be feasible to search for capillary critical points, at which $(\partial H/\partial f)_\mu = (\partial^2 H/\partial f^2)_\mu = 0$, provided these occur at large H so they are not masked by oscillations. This requires high temperatures and small undersaturations.

Finally we return to real porous material and the adsorption isotherm sketched in Fig. 1. While such behavior is found for a wide variety of materials the detailed shape of the (reversible) hysteresis loop often differs significantly between different materials.[1] It is often the case that the hysteresis loops disappear at high temperature so that Γ then increases monotonically with p/p_{sat}. Explanations of the hysteresis abound,[1,3,4] most of which we find unconvincing. For the idealized single slit-like pore we considere here, the *equilibrium* adsorption isotherm simply exhibits a vertical jump at the first order transition, but hysteresis could certainly be associated with the *metastable* portions of the loops in $\Gamma(\mu)$ shown in Fig. 12(a). Thus one might find adsorption along a path *ABCD* and desorption along *DCEA*. Other, similar, paths are possible, but in each case the unstable region with $(\partial\Gamma/\partial\mu) < 0$ is excluded. The desorption path would always lie above the absorption path, as is found in experiment (see Fig. 1). This mechanism for hysteresis is equivalent to that described by Hill.[10] Our numerical results (Figs. 19 and 20) show that the loops in Γ take a different form above and below T_w. In the complete wetting case (Fig. 19) the capillary spinodal point $\mu = \mu_1$ occurs for $p < p_{sat}$, whereas in a

partial wetting case (Fig. 20) the loop extends to $p > p_{sat}$.[49] In almost all experimental studies of gas adsorption in mesoporous solids complete wetting is assumed, i.e., the contact angle $\theta = 0$, so that the first case is probably more relevant to experiment. The adsorption loops need not be symmetrical about the first-order transition; there is no equal area construction for $\Gamma(\mu)$ or $\Gamma(p)$. Figure 9 suggests that the low pressure (density) metastable portion can be smaller than the high pressure (density) metastable portion, implying that desorption from liquid to gas can only occur close to the equilibrium transition, whereas adsorption can occur for pressures substantially in excess of that associated with the transition. Such asymmetry could lead to hysteresis loops with the shape sketched in Fig. 1. Moreover increasing the temperature, at fixed H, will drive the system to the line of critical points and, eventually, into the supercritical one-phase region with no loops and, therefore, no hysteresis. Thus it is tempting to infer that the hysteresis observed in experiments does arise from the mechanism we have outlined. In practice the solid will contain pores with a distribution of sizes and complex connectivity and presumably this smears out the hysteresis loops. While particular geometries (curious conical and "ink-bottle" capillaries are described in the literature[1]) might favor the development of certain metastable states and influence the shape of the loops, the underlying physical mechanism should remain the same as that described here for a single slit.[50] Cylinders should constitute a more realistic model for pores and density functional calculations are in progress for these. Preliminary results[52] suggest some important quantitative differences between cylinders and slits, but the qualitative features of the adsorption isotherms are the same. It is likely that fairly detailed comparison between theory and experiment will soon be possible and this should shed more light on the origin of the hysteresis.

In conclusion we believe we have provided satisfactory answers to several of the questions posed at the beginning of this paper.

ACKNOWLEDGMENTS

We have benefited from discussions with D. H. Everett and S. Lubetkin. This research was supported by S.E.R.C. (U.K.) and CAICYT (Spain). We are grateful to the British Council for travel funds.

APPENDIX A: DERIVATION OF EQUATION FOR THE CAPILLARY SPINODAL

Differentiating each side of Eq. (16) with respect to μ_h^M at fixed μ and T we obtain

$$\frac{\lambda}{2}\left(\frac{\partial H}{\partial \mu_h^M}\right) = (\psi(\mu_h^M) - \Delta p)^{-1/2} - \left(\frac{\partial \mu_h^w}{\partial \mu_h^M}\right)(\psi(\mu_h^w) - \Delta p)^{-1/2} + \frac{1}{2}\left(\frac{\partial \Delta p}{\partial \mu_h^M}\right)\int_{\mu_h^w}^{\mu_h^M} d\mu_h (\psi(\mu_h) - \Delta p)^{-3/2}, \tag{A1}$$

where there is an implicit + or − sign associated with each square root. We note that the first and third terms on the right-hand-side of Eq. (A1) are singular, but their sum is regular. Using the identity

$$(\psi(\mu_h) - \Delta p)^{-3/2} = -2\frac{\partial}{\partial \mu_h}((\psi(\mu_h) - \Delta p)^{-1/2})\left(\frac{\partial \psi(\mu_h)}{\partial \mu_h}\right)^{-1}, \tag{A2}$$

we can integrate by parts in Eq. (A1) to obtain

$$\frac{\lambda}{2}\left(\frac{\partial H}{\partial \mu_h^M}\right) = (\psi(\mu_h^M) - \Delta p)^{-1/2} - \left(\frac{\partial \mu_h^w}{\partial \mu_h^M}\right)(\psi(\mu_h^w) - \Delta p)^{-1/2} - \left(\frac{\partial \Delta p}{\partial \mu_h^M}\right)\left[(\psi(\mu_h^M) - \Delta p)^{-1/2}\left(\frac{\partial \psi(\mu_h^M)}{\partial \mu_h^M}\right)^{-1}\right.$$
$$\left. - (\psi(\mu_h^w) - \Delta p)^{-1/2}\left(\frac{\partial \psi(\mu_h^W)}{\partial \mu_h^w}\right)^{-1}\right] - \left(\frac{\partial \Delta p}{\partial \mu_h^M}\right)\int_{\mu_h^w}^{\mu_h^M} d\mu_h (\psi(\mu_h^M) - \Delta p)^{-1/2}\frac{\partial^2 \psi(\mu_h)}{\partial \mu_h^2}\left(\frac{\partial \psi(\mu_h)}{\partial \mu_h}\right)^{-2}. \tag{A3}$$

Since $\psi(\mu_h^M) = \Delta p$ [Eq. (17)], the singular first and third terms on the right-hand-side cancel. The derivative $(\partial \mu_h^w / \partial \mu_h^M)$ can be obtained by differentiating the boundary condition (19),

$$\frac{\partial \psi(\mu_h^w)}{\partial \mu_h^w}\left(\frac{\partial \mu_h^w}{\partial \mu_h^M}\right) - \left(\frac{\partial \Delta p}{\partial \mu_h^M}\right) - 2(\mu_h^w - \mu - 2\epsilon_w)\left(\frac{\partial \mu_h^w}{\partial \mu_h^M}\right) = 0.$$

Thus,

$$\left(\frac{\partial \mu_h^w}{\partial \mu_h^M}\right) = \left(\frac{\partial \Delta p}{\partial \mu_h^M}\right)\Big/\left(\frac{\partial \psi(\mu_h^w)}{\partial \mu_h^W} - 2(\mu_h^w - \mu - 2\epsilon_w)\right). \tag{A4}$$

Substituting this result in Eq. (A3) we find

$$\frac{\lambda}{2}\left(\frac{\partial H}{\partial \mu_h^M}\right) = \left(\frac{\partial \Delta p}{\partial \mu_h^M}\right)\left[(\psi(\mu_h^w) - \Delta p)^{-1/2}\left\{\frac{1}{2(\mu_h^w - \mu - \alpha\rho^w)} + \frac{1}{2(\alpha\rho^w - 2\epsilon_w)}\right\}\right.$$
$$\left. - \int_{\mu_h^w}^{\mu_h^M} d\mu_h (\psi(\mu_h) - \Delta p)^{-1/2}\frac{\partial^2 \psi(\mu_h)}{\partial \mu_h^2}\left(\frac{\partial \psi(\mu_h)}{\partial \mu_h}\right)^{-2}\right], \tag{A5}$$

where $\rho^w \equiv \rho(\mu_h^w)$ is the density at the wall. The vanishing of the right-hand-side then determines the capillary spinodal.

APPENDIX B: DERIVATION OF EQUATION FOR $\partial \mu_h(x)/\partial \mu$

Equation (14) may be reexpressed as

$$x = \pm \int_{\mu_h^w}^{\mu_h(x)} d\mu_h (\psi(\mu_h) - \Delta p)^{-1/2}, \tag{B1}$$

where $\mu_h(x) \equiv \mu_h(\rho(x))$. We consider the total derivative

$$\frac{dx}{d\mu} = \frac{\partial x}{\partial \mu} + \left(\frac{\partial x}{\partial \mu_h}\right)_\mu \left(\frac{\partial \mu_h}{\partial \mu}\right) + \left(\frac{\partial x}{\partial \mu_h^w}\right)_\mu \left(\frac{\partial \mu_h^w}{\partial \mu}\right)_{\mu_h^M} + \left(\frac{\partial x}{\partial \mu_h^M}\right)_\mu \left(\frac{\partial \mu_h^M}{\partial \mu}\right) + \left(\frac{\partial x}{\partial \mu_h^w}\right)_\mu \left(\frac{\partial \mu_h^w}{\partial \mu_h^M}\right)_\mu \left(\frac{\partial \mu_h^M}{\partial \mu}\right),$$

where the third term on the right-hand side refers to fixed μ_h^M. Using Eq. (B1) it follows that for fixed distance x and temperature T:

$$\frac{\partial x}{\partial \mu} + \left(\frac{\partial \mu_h(x)}{\partial \mu}\right)(\psi(\mu_h) - \Delta p)^{-1/2} - \left(\frac{\partial \mu_h^w}{\partial \mu}\right)_{\mu_h^M} (\psi(\mu_h^w) - \Delta p)^{-1/2}$$

$$+ \left(\frac{\partial \mu_h^M}{\partial \mu}\right)\left[\frac{1}{2}\left(\frac{\partial \Delta p}{\partial \mu_h^M}\right)_\mu \int_{\mu_h^w}^{\mu_h(x)} d\mu_h (\psi(\mu_h) - \Delta p)^{-3/2} - \left(\frac{\partial \mu_h^w}{\partial \mu_h^M}\right)_\mu (\psi(\mu_h^w) - \Delta p)^{-1/2}\right] = 0. \tag{B2}$$

Again the + or − sign is implicit in each square root. As in Appendix A certain terms in Eq. (B2) are singular in the limit $x \to \lambda H/2$. Using Eq. (A2) and integrating by parts, we obtain

$$\frac{\partial x}{\partial \mu} + \left(\frac{\partial \mu_h(x)}{\partial \mu}\right)(\psi(\mu_h) - \Delta p)^{-1/2} - \left(\frac{\partial \mu_h^w}{\partial \mu}\right)_{\mu_h^M}(\psi(\mu_h^w) - \Delta p)^{-1/2} + \left(\frac{\partial \mu_h^M}{\partial \mu}\right)\Bigg[- \left(\frac{\partial \Delta p}{\partial \mu_h^M}\right)_\mu \Bigg\{(\psi(\mu_h) - \Delta p)^{-1/2}\left(\frac{\partial \psi}{\partial \mu_h}\right)^{-1}$$

$$- (\psi(\mu_h^w) - \Delta p)^{-1/2}\left(\frac{\partial \psi(\mu_h^w)}{\partial \mu_h^w}\right)^{-1} + \int_{\mu_h^w}^{\mu_h(x)} d\mu_h (\psi(\mu_h) - \Delta p)^{-1/2}\left(\frac{\partial^2 \psi}{\partial \mu_h^2}\right)\left(\frac{\partial \psi}{\partial \mu_h}\right)^{-2}\Bigg\}$$

$$- \left(\frac{\partial \mu_h^w}{\partial \mu_h^M}\right)_\mu (\psi(\mu_h^w) - \Delta p)^{-1/2}\Bigg] = 0. \tag{B3}$$

Using Eqs. (13) and (17) we find

$$\frac{\partial x}{\partial \mu} = -\frac{1}{2}\int_{\mu_h^w}^{\mu_h(x)} d\mu_h (\psi(\mu_h) - \Delta p)^{-3/2} \frac{\partial}{\partial \mu}(\psi(\mu_h) - \psi(\mu_h^M)) = \int_{\mu_h^w}^{\mu_h(x)} d\mu_h (\psi(\mu_h) - \Delta p)^{-3/2}(\mu_h - \mu_h^M) \tag{B4}$$

which is regular as $x \to \lambda H/2$. We note that the fourth term in Eq. (B3) reduces to $-(\partial \mu_h^M/\partial \mu)(\psi(\mu_h^M) - \Delta p)^{-1/2}$ in the limit $x \to \lambda H/2$ and that this cancels with the second term in the same limit. By comparing Eqs. (A3) and (B3) we find that in the limit $x \to \lambda H/2$ the coefficient of $(\partial \mu_h^M/\partial \mu)$ is precisely $\frac{1}{2}\lambda (\partial H/\partial \mu_h^M)_\mu$. Equation (B3) then reduces to

$$\frac{\lambda}{2}\left(\frac{\partial H}{\partial \mu}\right) - \left(\frac{\partial \mu_h^w}{\partial \mu}\right)_{\mu_h^M}(\psi(\mu_h^w) - \Delta p)^{-1/2} + \frac{\lambda}{2}\left(\frac{\partial H}{\partial \mu_h^M}\right)_\mu \left(\frac{\partial \mu_h^M}{\partial \mu}\right) = 0 \tag{B5}$$

which is equivalent to $dH/d\mu = 0$. The derivative $(\partial \mu_h^w/\partial \mu)_{\mu_h^M}$ may be evaluated by differentiating the boundary condition Eq. (19):

$$\frac{\partial}{\partial \mu}(\psi(\mu_h^w) - \Delta p) = 2(\mu_h^w - \mu - 2\epsilon_w)\left(\frac{\partial \mu_h^w}{\partial \mu} - 1\right).$$

The left-hand side is $(\partial/\partial \mu)(\psi(\mu_h) - \psi(\mu_h^M)_{\mu_h = \mu_h^w} + \left(\frac{\partial \mu_h^w}{\partial \mu}\right)(\partial \psi/\partial \mu_h)_{\mu_h = \mu_h^w}$ which reduces to $-2(\mu_h^w - \mu_h^M) + 2(\mu_h^w - \mu - \alpha \rho^w)(\partial \mu_h^w/\partial \mu)$.

It follows that

$$\left(\frac{\partial \mu_h^w}{\partial \mu}\right) = \frac{\mu_h^M - \mu - 2\epsilon_w}{\alpha \rho^w - 2\epsilon_w}, \tag{B6}$$

where ρ^w is the density at the wall. Equations (B4) and (B6) indicate that the first two terms in Eq. (B5) are finite but nonzero. [We do not consider the special cases that arise when the numerator or denominator of Eq. (B6) vanishes.] Consequently, if $(\partial H/\partial \mu_h^M)_\mu = 0$, as occurs at a capillary critical point or spinodal [Eq. (B5)] implies that $(\partial \mu_h^M/\partial \mu) \to \infty$. This is equivalent to a divergence of the midpoint compressibility or susceptibility.

Equation (B3) can be rewritten as

$$\left(\frac{\partial \mu_h(x)}{\partial \mu}\right)(\psi(\mu_h)-\Delta p)^{-1/2}=\frac{(\mu_h^M-\mu-2\epsilon_w)}{\alpha\rho^w-2\epsilon_w}(\psi(\mu_h^w)-\Delta p)^{-1/2}+\int_{\mu_h^w}^{\mu_h(x)}d\mu_h\,\frac{(\mu_h^M-\mu_h)}{(\psi(\mu_h)-\Delta p)^{3/2}}$$
$$+\left(\frac{\partial \mu_h^M}{\partial \mu}\right)\left[(\mu_h^M-\mu-\alpha\rho^M)\left\{\frac{(\psi(\mu_h(x))-\Delta p)^{-1/2}}{\mu_h(x)-\mu-\alpha\rho(x)}-\frac{(\psi(\mu_h^w)-\Delta p)^{-1/2}}{\mu_h^w-\mu-\alpha\rho^w}\right.\right.$$
$$\left.+2\int_{\mu_h^w}^{\mu_h(x)}d\mu_h(\psi(\mu_h)-\Delta p)^{-1/2}\frac{\partial^2\psi}{\partial\mu_h^2}\left(\frac{\partial\psi}{\partial\mu_h}\right)^{-2}\right\}$$
$$\left.-\frac{(\mu_h^M-\mu-\alpha\rho^M)}{\alpha\rho^w-2\epsilon_w}(\psi(\mu_h^w)-\Delta p)^{-1/2}\right], \tag{B7}$$

where we have used the result $(\partial\Delta p/\partial\mu_h^M)=2(\mu_h^M-\mu-\alpha\rho^M)$ and Eq. (A4). In the limit $H\to\infty$ $(\Delta p\to 0)$ $\mu_h^M\to\mu_h^b$, the bulk hard sphere chemical potential so that $\mu_h^M-\mu-\alpha\rho^M\to 0$, and the term in square brackets vanishes provided x remains finite. The sum of the first two terms on the right-hand side can be shown to be equivalent to the right-hand side of Eq. (A6) of Ref. 31. It is these terms which give rise to a divergence of $(\partial\mu_h(x)/\partial\mu)$ in the limit of complete wetting. For finite H the wetting film is of finite thickness and this type of divergence does not occur. The divergence of $(\partial\mu_h^M/\partial\mu)$ at the capillary critical point is associated with the vanishing of the sum of the other terms in Eq. (B7).

[1] S. J. Gregg and K. S. W. Sing, *Adsorption, Surface Area, and Porosity* (Academic, New York, 1982), Chap. 3.

[2] A. Zsigmondy, Z. Anorg. Chem. **71**, 356 (1911).

[3] For a review, see D. H. Everett and J. M. Haynes, in *Colloid Science, Vol. 1 Specialist Periodicals Reports* (Chemical Society, London, 1973), p. 123.

[4] L. H. Cohan, J. Am. Chem. Soc. **60**, 433 (1938). Cohan also proposed an explanation for hysteresis of the adsorption involving the difference in mean radius of curvature between a "full" cylindrical capillary with a hemispherical meniscus and that of an "empty" capillary with only a cylindrical wetting film. This explanation has persisted in the literature (see Ref. 1), but has not been supported by theory.

[5] B. V. Derjaguin, Zh. Fiz. Khim. **14**, 137 (1940). [English translation in Acta Physicochim. URSS **12**, 181 (1940).] Derjaguin also recognized the connection between the phenomena of capillary rise and condensation and derived explicit formulae for both which include the effects of long-ranged forces and wetting films.

[6] This is discussed further by R. Evans and U. Marini Bettolo Marconi, Chem. Phys. Lett. **114**, 415 (1985) who recover Derjaguin's results from a modern density functional approach.

[7] J. C. P. Broekhoff and J. H. de Boer, J. Catal. **9**, 8 (1967).

[8] M. W. Cole and W. F. Saam, Phys. Rev. Lett. **32**, 985 (1974); W. F. Saam and M. W. Cole, Phys. Rev. B **11**, 1086 (1975).

[9] (a) D. Nicholson, J. Chem. Soc. Faraday Trans. 1 **72**, 29 (1976); (b) D. Nicholson and N. G. Parsonage, *Computer Simulation and the Statistical Mechanics of Adsorption* (Academic, New York, 1982), Chap. 7. 4.

[10] T. L. Hill, J. Chem. Phys. **15**, 767 (1947).

[11] D. Nicholson, J. Chem. Soc. Faraday Trans. 1 **71**, 239 (1975).

[12] B. V. Derjaguin and N. V. Churaev, J. Colloid Interface Sci. **54**, 157 (1976). We are grateful to Dr. Churaev for bringing this paper to our attention.

[13] W. van Megen and I. K. Snook, Mol. Phys. **54**, 741 (1985).

[14] J. E. Lane and T. H. Spurling, Aust. J. Chem. **33**, 231 (1980).

[15] J. E. Lane and T. H. Spurling, Aust. J. Chem. **34**, 1529 (1981).

[16] B. C. Freasier and S. Nordholm, J. Chem. Phys. **79**, 4431 (1983).

[17] See, for example, H. Nakanishi and M. E. Fisher, J. Chem. Phys. **78**, 3279 (1983), and references therein.

[18] J. Chalupa and B. A. Huberman, J. Chem. Phys. **72**, 5276 (1980).

[19] R. Lipowsky and G. Gompper, Phys. Rev. B **29**, 5213 (1984); see their Eq. (7).

[20] D. Sornette, Phys. Rev. B **31**, 4672 (1985).

[21] P. Sheng, Phys. Rev. A **26**, 1610 (1982).

[22] See, for example, J. S. Rowlinson and B. Widom, *Molecular Theory of Capillarity* (Oxford University, Oxford, 1982) and Ref. 9(b).

[23] For a comprehensive review, see D. E. Sullivan and M. M. Telo da Gama, in *Fluid Interfacial Phenomena*, edited by C. A. Croxton (Wiley, New York, 1985).

[24] D. E. Sullivan, Phys. Rev. B **20**, 3991 (1979).

[25] D. E. Sullivan, J. Chem. Phys. **74**, 2604 (1981).

[26] Some preliminary results for the partial wetting case were published earlier, R. Evans and P. Tarazona, Phys. Rev. Lett. **52**, 557 (1984).

[27] This argument is equivalent to that of Cohan (Ref. 4).

[28] We shall find that the terms liquid and gas are somewhat misleading when we approach a critical point.

[29] See, for example, R. Evans, Adv. Phys. **28**, 143 (1979).

[30] It can be shown that $H_{co}=2a^{-1}$ arctan (a^{-1}) with $a^2=-\frac{1}{2}(\partial^2\psi/\partial\mu_h^2)_{\mu_h=\mu_h(\bar{\rho})}$.

[31] P. Tarazona and R. Evans, Mol. Phys. **47**, 1033 (1982). See Eq. (44).

[32] An equivalent result is given by Eq. (11) of Ref. 19.

[33] Equation (33) is equivalent to the condition for a critical point employed in Ref. 17.

[34] See, for example, Ref. 31.

[35] $H_t\approx 18$Å, or approximately 5.3 atomic diameters, in Ref. 14. For $12\lesssim H<18$Å, Γ increases almost linearly with H. For smaller values of H the deviations from linearity are more pronounced. Short-ranged correlations become more important at these small separations.

[36] See Fig. 7 of Ref. 16.

[37] S. G. Ash, D. H. Everett, and D. Radke, J. Chem. Soc. Faraday Trans. 2 **69**, 1256 (1973).

[38] Calculations were also performed for $\epsilon_w=4.5T_c$ which has $T_W\approx 0.57\ T_c$. For $T=0.8T_c$ and $T=0.9T_c$ the coexistence curves and the capillary critical points are shifted to much larger undersaturations than those shown in Fig. 15 for $T>T_W$. The unmodified Laplace equation is reasonably accurate for $\lambda H\gtrsim 100$ corresponding to undersaturations of 2% or less.

[39] In the slab approximation the profile contains no information about the (bulk)correlation length; critical scaling is not included. Consequently the approximation is more appropriate to lower temperatures.

[40] Such a result was also obtained in Ref. 17.

[41] M. R. Moldover and R. W. Gammon, J. Chem. Phys. **80**, 528 (1984).

[42] For very small values of ϵ_w a transition to complete wetting by gas (drying) occurs at a single wall (see Refs. 24 and 25). We do not consider this case here.

[43] J. W. Cahn, J. Chem. Phys. **66**, 3667 (1977).

[44] C. Ebner and W. F. Saam, Phys. Rev. Lett. **38**, 1486 (1977).

[45] R. Evans and U. Marini Bettolo Marconi, Phys. Rev. A (to be published). Coexisting thick and thin films only occur as the stable configurations for rather small values of $1/H$. We find that the stable prewetting surface lies inside the condensation surface shown here in Fig. 21. The surfaces intersect in a line of triple points.

[46] See, for example, P. G. deGennes, J. Phys. (Paris) **42**, L377 (1981); R. Pandit, M. Schick, and M. Wortis, Phys. Rev. B **26**, 5112 (1982); P. Tarazona and R. Evans, Mol. Phys. **48**, 799 (1983); M. P. Nightingale, W. F. Saam, and M. Schick, Phys. Rev. Lett. **51**, 1275 (1983); P. Tarazona, M. M. Telo da Gama, and R. Evans, Mol. Phys. **49**, 283, 301 (1983); R. Lipowsky, Phys. Rev. Lett. **52**, 1429 (1983).

[47] Density functional theories which go beyond the local density approximation for hard spheres have been developed and applied successfully to studies of adsorption and freezing [see, for example, P. Tarazona and R. Evans, Mol. Phys. **52**, 847 (1984) and P. Tarazona, Phys. Rev. A **31**, 2672 (1985)]. We are currently applying these approaches to fluids in capillaries. Preliminary results for the same potential functions indicate the surface tensions differ quantitatively from those calculated here and the tem-

peratures T_W and T_s are lower than those given here. This implies that the coexistence lines and critical points remain at $p < p_{sat}$ for substantially lower temperatures than those shown in Fig. 15.

[48]See, for example, R. G. Horn and J. N. Israelachvili, Chem. Phys. Lett. **71**, 192 (1980).

[49]The situation is somewhat different when the wetting transition is first order. The gas can extend to $p > p_{sat}$ if $T_W < T < T_{sc}$, where T_{sc} is the critical temperature of the prewetting transition (see Ref. 45). This corresponds to a thin film. If $T > T_{sc}$ thick films develop and $\mu_1 < \mu_{sat}$ as is described here.

[50]An identical viewpoint was taken by Hill in Ref. 10. In the literature, however, see, for example, Refs. 1, 3, 4, and 7, there is much confusion concerning the effect of pore geometry on hysteresis. Certain geometries are supposed not to exhibit hysteresis while others are. For us there is no doubt that for a pore of any reasonable geometry an equilibrium first-order transition with a single vertical jump in the adsorption should occur. This will be accompanied by metastable states and hysteresis. The confusion lies in the use of macroscopic arguments which do not properly recognize the underlying character of capillary condensation.

[51]A. M. Nemirovsky, Zhen-gang Wang, and K. F. Freed (to be published).

[52]R. Evans, U. Marini Bettolo Marconi, and P. Tarazona, J. Chem. Soc. Faraday Trans. (to be published).